Fluvio-deltaic response to relative sea-level fall: A case study of the Goose River delta, Labrador, Canada

Author: Austin Nijhuis

Boston College

The Graduate School of Arts and Sciences

Department of Earth and Environmental Sciences

FLUVIO-DELTAIC RESPONSE TO RELATIVE SEA-LEVEL FALL: A CASE STUDY OF THE GOOSE RIVER DELTA, LABRADOR, CANADA

a thesis

by

AUSTIN GERRIT NIJHUIS

submitted in partial fulfillment of the requirements

for the degree of

Master of Science

December, 2013

Abstract

Fluvio-deltaic response to relative sea-level fall: a case study of the Goose River delta, Labrador, Canada

Austin Nijhuis

Advisor: Douglas Edmonds

Due to their low-lying position near the shoreline, river deltas are vulnerable to fluctuations in relative sea-level (RSL). Moreover, relatively little is known about fluvio-deltaic dynamics during RSL fall because the resulting deposits have low preservation potential. In this paper, I present a field-based study of the Goose River delta, coupled with numerical model simulations, that investigates the fluvio-deltaic response to RSL fall. The Goose River delta is a sandy fjord delta at the mouth of the Goose River located at the western end of Lake Melville, an inlet of the Labrador Sea, Canada and has experienced a RSL fall of 3 to 6 mm/yr in the past 5000 years due to post-glacial isostatic rebound. Aerial images show three abandoned delta lobes and one active lobe, suggesting that avulsions and lobe-switching occurred during RSL fall. Elevation analysis using Shuttle Radar Topography Mission (SRTM) digital elevation model (DEM) data and optically-stimulated luminescence (OSL) dating suggest that a series of downstepping terraced delta lobes formed at the mouth of the Goose River during a period of RSL fall. Similarly, Delft3D model runs show continued avulsions and formation of multiple terraced delta lobes deposited at progressively lower elevations. I show computationally that by decreasing delta lobe widths, deltas may remain aggradational during RSL fall, creating conditions favorable for lobe-switching during RSL fall. Observations from the field and model runs provide a critical link in understanding the geomorphic processes

occurring during RSL fall, and in particular show that 1) incision and sediment bypass is not a necessary response to RSL fall and 2) lateral migration of a delta via avulsion can continue to occur with falling sea-level.

Table of Contents

Acknowledgements

I would like to acknowledge and thank everyone who helped make this research possible. I would especially like to thank my advisor, Douglas Edmonds, who provided support and guidance with my work and helped me grow into a more intelligent and capable researcher. Without him, none of this work would be possible (obviously).

I would also like to thank everyone from the Goose Bay research team from Indiana University, Pennsylvania State University, University of Illinois Urbana-Champaign, and the University of Hull and the other members of my thesis committee, Gail Kineke and Noah Snyder.

Lastly, I would like to thank my family, fellow graduate students, and friends. You helped me both complete this thesis and procrastinate (special thanks for this). I couldn't have done this without you.

List of Figures

List of Tables

1. Introduction

Understanding the fluvio-deltaic response to fluctuations in relative sea-level (RSL) is of central importance to hydrocarbon exploration, predicting reservoir properties, and linking past climate conditions with the stratigraphic record (Blum and Tornqvist, 2000). Relatively little is known about how RSL fall modifies fluvio-deltaic processes due to difficulties associated with interpreting ancient stratigraphy (Paola, 2000) and the dearth of modern examples of deltas experiencing RSL fall. Standard sequence-stratigraphic models rely on the graded stream concept and link RSL fall with degradation of river systems and the formation of incised valleys that cease to laterally migrate (e.g. Vail et al, 1977; Posamentier et al., 1998). In contrast, recent geomorphic models suggest a time-lag between the onset of RSL fall and degradation, allowing for continued aggradation over long periods of time (Leeder and Stewart, 1996; van Heijst and Postma, 2001; Swenson and Muto, 2007). In particular, it remains unclear how a fluvio-deltaic system can continue to laterally migrate via avulsion, an aggradational process (i.e. Slingerland and Smith, 2004), during RSL fall. Recent experiments suggest that avulsions are possible during RSL fall, but confirmation is difficult without empirical geomorphic evidence combined with well-defined age constraints (Meijer, 2002; Strong and Paola, 2008).

In this paper, we examined the fluvio-deltaic processes occurring during RSL fall through a case study of the Goose River delta, a modern delta experiencing RSL fall. The delta is an ideal site to investigate the fluvio-deltaic response to RSL fall because of its RSL history, preserved delta lobes, and relatively low influence of external forces that can affect delta growth, such as waves, tides, and buoyancy (Wright and Coleman, 1973;

Wright, 1977). Aerial images suggest that the Goose River delta avulsed multiple times during a period of known RSL fall, resulting in the formation of multiple delta lobes. To determine the depositional history of the Goose River delta lobes, we extracted Shuttle Radar Topography Mission (SRTM) digital elevation model (DEM) data from each lobe and collected samples for optically-stimulated luminescence (OSL) dating. Goose River delta observations were coupled with a physics-based morphodynamic model to determine how a river such as the Goose River may evolve during RSL fall. With this approach, we were able to link the underlying fluvio-deltaic processes occurring during RSL fall with empirical geomorphic evidence.

2. Background

The role of RSL fall on fluvio-deltaic systems has received considerable attention in both sequence stratigraphy and geomorphology (Blum and Tornqvist, 2000). Long-standing conceptual models of the fluvio-deltaic response to fluctuations in RSL are based on early graded stream studies (eg. Fisk, 1944; Mackin, 1948; Lane, 1955). A stream in equilibrium (i.e. 'graded') should degrade in response to falling RSL and aggrade with RSL rise due to changes in water surface slope (Vail, et al., 1977; Posamentier, et al., 1988). Degradation during RSL fall results in rapid progradation of the shoreline and the formation of incised valleys. Due to the long time associated with fluvio-deltaic evolution and the dearth of modern deltas undergoing RSL fall, these models remain largely untested.

Relying on the graded stream response described above, sequence stratigraphic concepts assume that during RSL fall, rivers incise and produce correlative surfaces called sequence boundaries. Recent numerical and physical-scale models suggest that these sequence-stratigraphic models are oversimplified. In particular, these models suggest that river response to RSL fall differs from the sequence stratigraphic model in three ways. The first is that aggradation in the fluvial system can continue for a period of time during RSL fall. This occurs because river-system response is not instantaneous and the time-scale for the RSL fall signal to travel up the fluvial system can be long (Leeder and Stewart, 1996; van Heijst and Postma, 2001). The longitudinal profile of a fluvio-deltaic profile is lowered during RSL fall by an upstream-propagating knickpoint and the response time is a function of sediment supply and rate of relative sea-level fall (Swenson and Muto, 2007). Second, river avulsions and deltaic lobe-switching persist during RSL

fall (Schumm, et al., 1993; Koss et al., 1994; Wood et al., 1993). Using a numerical model, *Meijer* (2002) showed that sea-level fall results in rapid delta progradation and the development of multiple obliquely stacked delta lobes. Degradation was largely absent and only occurred after the delta prograded past the continental shelf. Avulsions continued at the sites of active delta lobes throughout sea-level fall. These observations largely agree with micro-scale flume experiments (Koss et al., 1994; van Heijst and Postma, 2001). Third, incised valleys observed in the stratigraphic record are likely composite erosional surfaces that are time-transgressive, rather than actual topographic valleys (Strong and Paola, 2008). *Strong and Paola* (2008) show a series of downstepping, unpaired delta-lobe terraces formed during continuous sea-level fall. However, the delta lobes were not preserved due to continuous incision and backfill during sea-level fall and subsequent rise, leading to the formation of incised valleys. These observations led the authors to question whether incised valleys, thought to be characteristic of RSL fall, were actually geomorphic features formed by the fluvial landscape.

These studies highlight that we are only beginning to understand the geomorphic and stratigraphic response of rivers and deltas to RSL fall. In particular, it is unclear how the process of river avulsion, which is a key process for the construction of fluvial stratigraphy, is modified by RSL fall. That avulsions should occur at all during RSL fall is counterintuitive, because they are thought to be the result of aggradation (Slingerland and Smith, 2004; Jones and Schumm, 2009). By this theory, alluviation of a channel leads to aggradation of channel levees, causing the channel to become superelevated, a condition where the channel bed has the same elevation as the adjacent floodplain.

Superelevation leads to avulsions because the cross-levee slope is steeper than the down-channel slope. Therefore, when flow exits the channel, it will preferentially flow down the floodplain. These theories have been developed for fluvial systems far from the coast undergoing no change in sea-level.

If we consider a fluvio-deltaic system experiencing RSL fall, things are considerably more complicated. Aggradation is likely occurring at a slower pace, if at all; this alone suggests avulsions should occur less frequently (e.g. Jerolmack and Mohrig, 2007). But during RSL fall the superelevation rate of channels in coastal systems may not be set by the in-channel aggradation rate as conceived of for fluvial systems far from the coast. Consider that during RSL fall, superelevation is the result of the aggradation rate in the channel, plus the RSL fall rate if it exposes steeper slopes, like delta foresets, for instance. Together these two processes may create alternate paths that attract channels causing avulsion.

Avulsion is one of the fundamental processes that create fluvio-deltaic stratigraphy and understanding its mechanism during RSL fall will lead to better prediction of deposits produced during RSL fall. Many fundamental questions remain unanswered: 1) How can a delta remain aggradational during RSL fall?; 2) how is avulsion frequency influenced by RSL fall?; and 3) what sets the scale of deltaic lobes produced by avulsion during RSL fall? While physical and numerical models support the idea of aggradation and avulsion during RSL, there is little corroborating evidence in the ancient stratigraphic record and few Quaternary examples given the present condition of eustatic sea-level rise. Further, it is unknown how well these models apply to real-world systems. Modern coastal areas currently experiencing RSL fall due to isostatic rebound

following deglaciation can serve as ideal settings to investigate RSL fall dynamics (Hart and Long, 1996).

3. Goose River delta field study

3.1 Overview of field setting

The Goose River study area (Figure 1) is an ideal site to investigate the fluvio-deltaic response to sea-level fall because of its preserved deltaic lobes, sea-level history and relatively low influence of external forces in Goose Bay that can affect delta growth, such as waves, tides, and buoyancy (Wright and Coleman, 1973; Wright, 1977). Goose Bay lies at the western end of Lake Melville, a fjord-type estuary located 200 km inland (Liverman, 1997). Lake Melville is connected to the Labrador Sea by The Narrows, a 50 m deep, 30 km long, 2 km wide channel (Vilks and Mudie, 1983). Tidal choking at The Narrows regulates the tidal signature entering Lake Melville. The tidal amplitude within Lake Melville is 0.4 m with a maximum of 0.7 m. Tidal currents vary from 0.05 to 1 m/s (Vilks et al., 1987). Salinity is controlled by an influx of freshwater from five major rivers and by a 28 m bottom sill at The Narrows that prevents saltwater from entering into the lake (Vilks and Mudie, 1983). Salinity decreases from 31 psu seaward of The Narrows to 5 – 10 psu in Goose Bay and vertical mixing of incoming freshwater with saline water is limited. Most of Goose Bay is between 20 m and 40 m deep with a maximum of 60 m; however, Goose Bay shallows nearshore to 10 m in Terrington Basin (Blake Jr., 1956).

The Goose River delta is located at the mouth of the Goose River and empties into Goose Bay near the town of Happy Valley-Goose Bay in Labrador, Canada (53.36° N, 60.38° W). The Goose River has a drainage area of 3,450 km^2 and flows into the western end of Goose Bay, known as Terrington Basin. In the study site, the Goose River is approximately 100 - 200 m wide and 2 - 3 m deep (based on surveys conducted in

2012). Modern hydrologic data on the Goose River is limited, nonetheless historical water discharges range from 5 (low flow) to 500 m^3/s (Coachman, 1953).

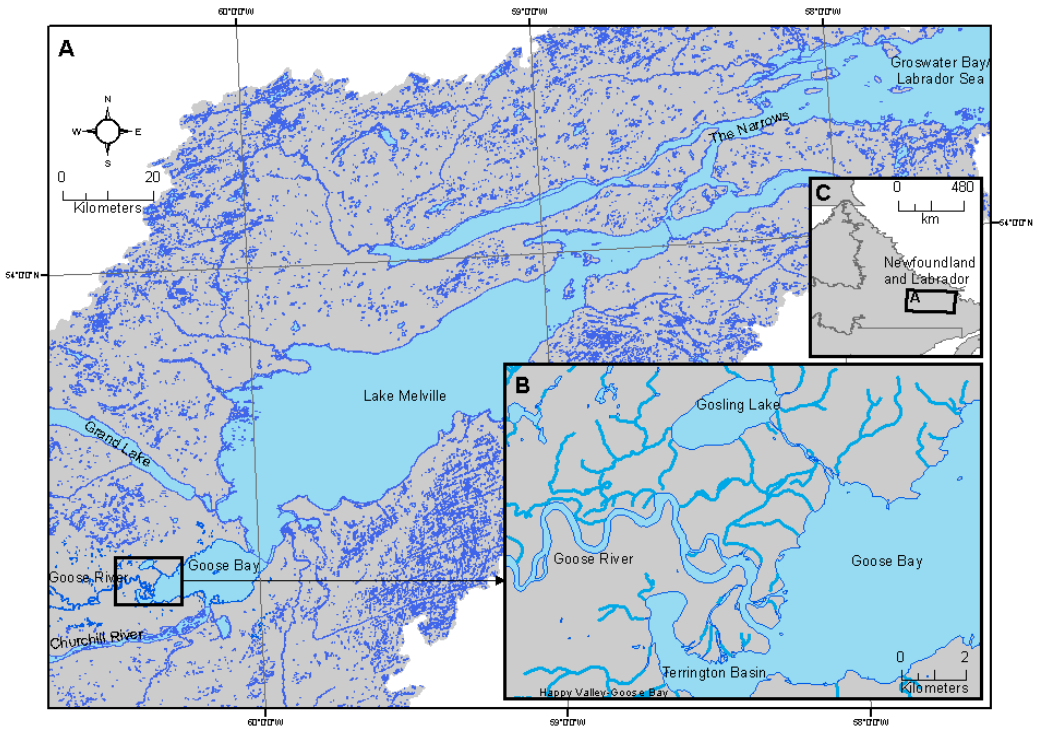

Figure 1. Map showing the location of (A) Lake Melville and its surrounding watersheds and (B) the Goose River/Goose Bay study area in Labrador, Canada (C). Source: Natural Resources Canada

There is geomorphic evidence for multiple deltaic lobes at the mouth of the Goose River. Relict channel networks and the lobate shape of at least four delta lobes deposited in different orientations are visible in aerial photographs (Figure 2, Figure 3). Three moribund lobes were deposited in the northwest (NWL), north (NL), and south (SL) and one lobe is currently depositing sediment towards the southeast (AL) at two positions. The orientation of the two northern lobes indicates that the Goose River once flowed into Lake Melville via Gosling Lake to the north prior to its current entry points (Figure 1; Liverman, 1997). Radiocarbon wood samples from these channels are dated 1390 years

(NWL) and 540 years (NL) before present (Newfoundland and Labrador Geological Survey, 2001).

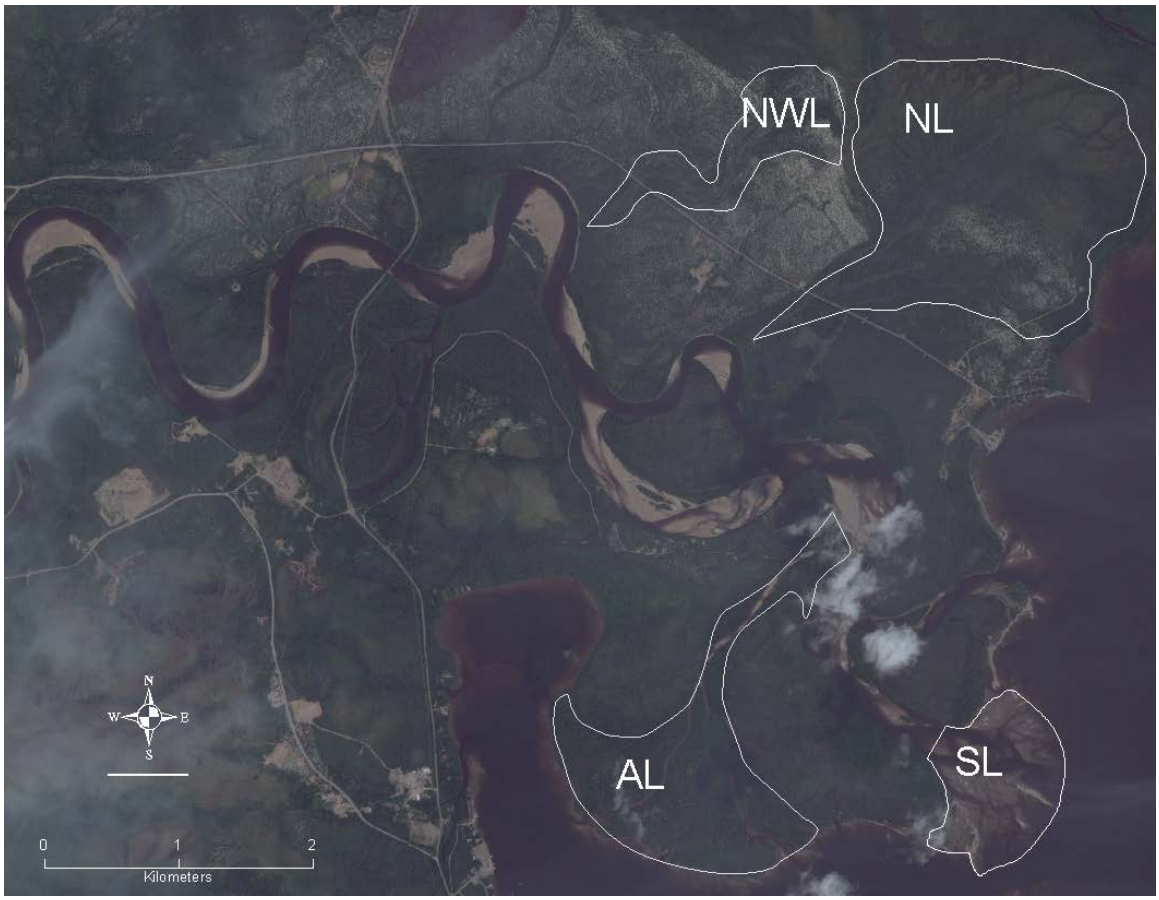

Figure 2. SPOT satellite image of the Goose River study area taken in June 2003. Source: Esri

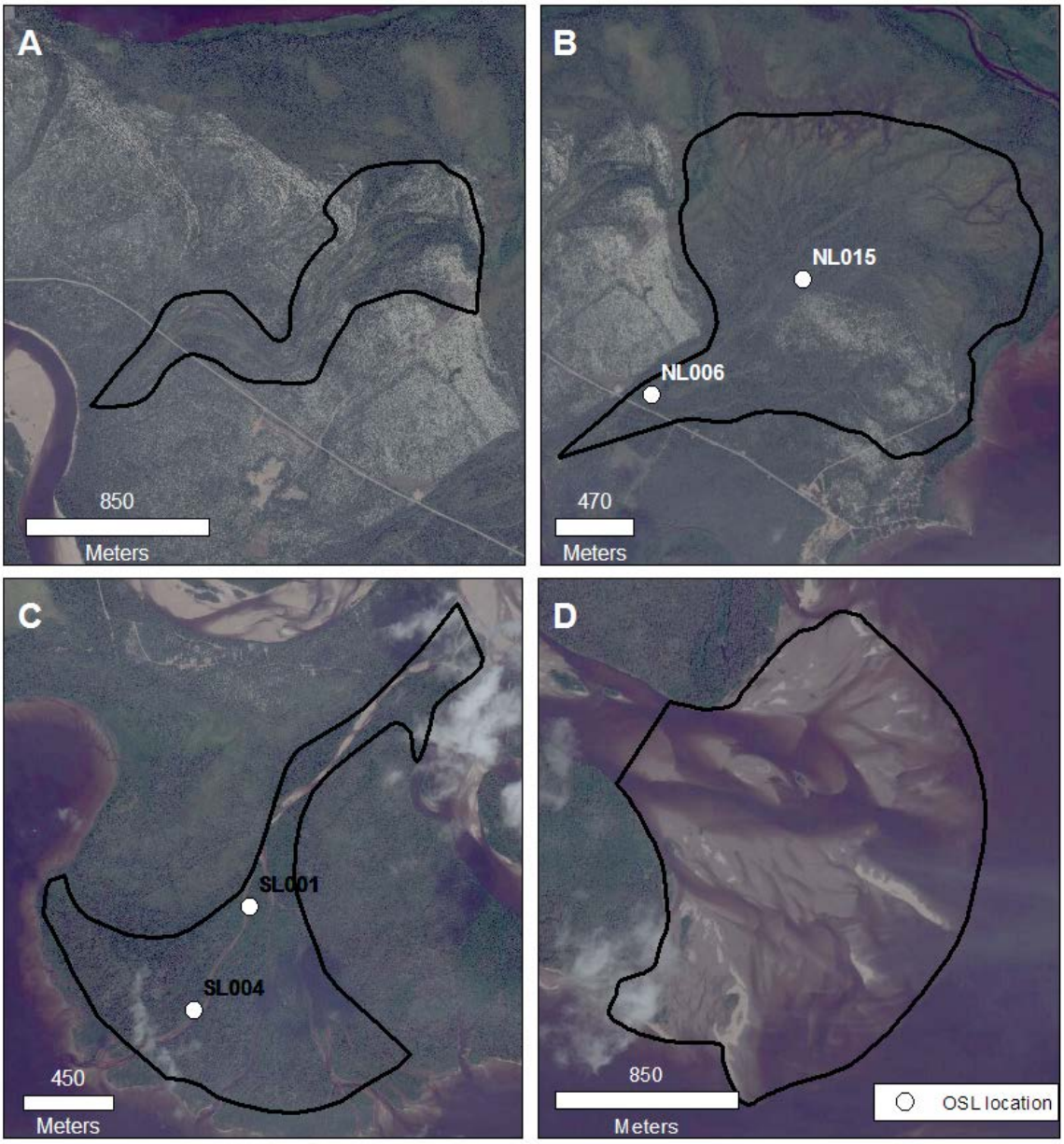

Figure 3. Detailed satellite images of the Goose River delta lobes: (A) NWL, (B) NL, (C) SL, and (D) AL. Deltaic land basinward of the dashed line in (C) has likely been modified by tides and/or ice. Satellite image, dated June 2003, was obtained from SPOT. Source: Esri

Quaternary sea-level and climate history

Two factors are important in the post-glacial sea-level history of the Goose Bay region: climatic changes and geomorphic modification of the landscape due to crustal movements (Fitzhugh, 1973). During the last glacial maximum, the Laurentide Ice Sheet covered most of the Canadian Shield. Ice sheet retreat during the Holocene occurred over three stages in the Lake Melville region: 1) initial ice margin retreat over Lake Melville tidewaters between 10 and 9 ka, 2) ablation on land between 6 and 9 ka resulting in the formation of paraglacial deltas, and 3) full ablation on land, resulting in an increase in organic carbon flux entering Lake Melville (< 6 ka) (Syvitski and Lee, 1993).

In response to ice-sheet retreat, much of the Labrador coast has undergone glacial isostatic rebound. At the same time, eustatic global sea-level has risen 120 to 140 m over the past 18 ka (Fairbanks, 1989); but the relative sea-level history (i.e. the combined effects of eustatic sea-level rise and glacial rebound) has resulted in a relative sea-level fall. RSL curves have been constructed for much of the Labrador coast based on geological mapping, age-dating of deposits, and archaeological investigations. The Goose Bay RSL curve was constructed by radiocarbon dating of geological materials associated with elevations of raised marine deposits and supplemented by dating of human artifacts from prehistoric coastal communities (Fitzhugh, 1973; Clark and Fitzhugh, 1993).

Marine deposits have been mapped at 135 m above sea-level (m a.s.l.) and given the timing of ice-sheet retreat at 7.5 ka, the initial response probably created some of the fastest RSL fall rates on the Labrador coast (Clark and Fitzhugh, 1993). An initial rapid period of elastic adjustment resulted in a RSL fall between 76 and 122 mm/yr. Over the past 5 ka, RSL has slowed to a current rate of <3 mm/yr, coinciding with delayed plastic

recovery (Fitzhugh, 1973). Radiocarbon dating of fossil trees found near Grand Lake (Figure 1) suggests a RSL fall rate of 4 mm/yr over the past 2 ka (Blake Jr., 1955), which is consistent with the work of *Fitzhugh* (1973) and *Clark and Fitzhugh* (1993). High-resolution, GPS-based geodynamic monitoring over the past two decades shows isostatic rebound rates near Goose Bay similar to those obtained by dating techniques (Henton, et al., 2006).

Following deglaciation, the Goose Bay region underwent climatic and vegetation changes. Pollen assemblages from sediment cores taken from Lake Melville show a transition from arctic tundra to boreal forest (Vilks and Mudie, 1983). Before 8 ka, low arctic tundra was present in the region. From 6.6 to 8 ka, shrub tundra occupied the region, indicating paraglacial conditions. Boreal forest was established by 6 ka. A lower boreal forest pollen concentration appeared about 4 ka, suggesting a regional climatic cooling. Sedimentation rates into Lake Melville were three to four times higher in the early postglacial phases of open tundra and shrub tundra, consistent with a fast initial rebound rate. A lower sedimentation rates corresponds with the onset of boreal forest 4 ka. *Vilks and Mudie* (1983) suggest that the decrease in sedimentation rate may reflect reduced erosion following the onset of vegetation of the Labrador highlands, but the reduced sedimentation rate also coincides with the transition from the fast to slow components of isostatic rebound, which altered valley gradients (Syvitski and Lee, 1993).

Previous radiocarbon dating work suggests that the four Goose River delta lobes in this study began to form approximately 2 ka (Newfoundland and Labrador Geological Survey, 2001), suggesting that the deltas formed following full ablation of the Laurentide Ice Sheet over Labrador (Syvitski and Lee, 1993). At this time, RSL was falling between

3 and 6 mm/yr (Blake Jr., 1956; Fitzhugh, 1973; Clark and Fitzhugh, 1992). Pollen assemblages suggest that the sedimentation rate entering Lake Melville was stabilized during this time due to the onset of boreal forest vegetation (Vilks and Mudie, 1983).

3.2 Methods

To understand how the Goose River delta responded to changes in RSL, geomorphic observations of the lower Goose River were made both in the field and remotely using aerial photographs and a DEM. Geomorphic observations were coupled with OSL dates to determine the depositional history of the Goose River delta. Hyrdologic and sedimentologic data were also collected in the field to use as initial and boundary conditions for numerical simulations.

Digital elevation model analysis

In addition to the active lobe, The Goose River has three extant lobes (Figure 3). To establish that the delta lobes are temporally distinct deposits formed during RSL fall, we conducted a DEM analysis of their elevations. The underlying assumption of this analysis is that if deltas were deposited during RSL fall, deltas of different ages should occupy distinct elevations related to different sea-level elevations. We used SRTM data to constrain the elevations of each delta lobe. SRTM data are near global, radar-derived elevation data collected during an 11-day survey on the Space Shuttle Endeavour in February 2000 that is useful for observing architectural elements in coastal and delta plains (Farr, et al., 2007; Syvitski, et al., 2012). SRTM data were available at 1 arc-second (~30 m) pixel resolution for the study area. Elevation accuracy depends on

location, terrain characteristics and surface features. Throughout North America, SRTM data have an average relative accuracy of 3 m (Berry et al., 2007). Accuracy is improved in relatively flat and homogenous floodplain regions, similar to the environments studied here, with a root mean square error (RMSE) of 1.55 m (Schumann et al., 2008). To assess the accuracy of SRTM data in our study area, we collected elevation points using a Leica Real-Time Kinematic (RTK) GPS Rover on two delta lobes (NL and SL) with vertical accuracy of less than 0.1 m.

Elevation data from four delta lobes were extracted from the SRTM DEM (Figure 4**)**. For the purpose of this analysis, a delta lobe is defined as the planform area that encompasses the distributary-channel network and closely associated overbank deposits. The upstream extent is defined by the intersection with the current Goose River. This definition is a minimum area because it only includes the area with obvious deltaic features and ignores those areas that may be deltaic, but have no deltaic expression in aerial photography. The relative accuracy of the SRTM DEM compared to the reference GPS data is expressed by the $RMSE_{DEM}$ metric:

$$RMSE_{DEM}=\sqrt{\frac{\sum_{i=1}^{n}(E_{GPS}-E_{SRTM})^2}{n_e}} \quad (3.1)$$

where $RMSE_{DEM}$ is the root mean square error between SRTM and GPS-derived elevations (m), E_{GPS} denotes the GPS-derived elevation (m), E_{SRTM} is the SRTM-derived elevation (m), and n_e is the total number of data points.

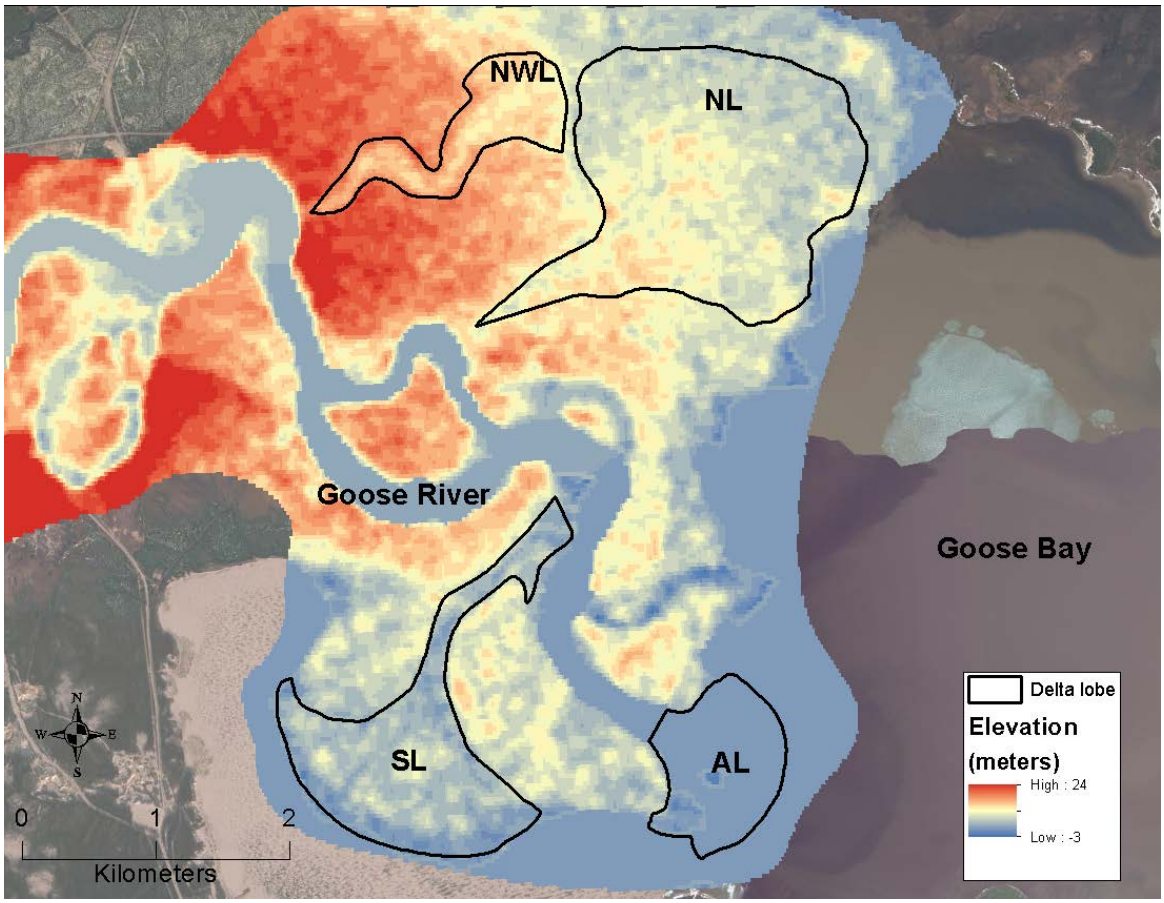

Figure 4. Map showing SRTM data for the lower Goose River overlain on a high-resolution satellite image. Delta lobes included in this study are outlined in black. Refer to Figure 6 for detailed SRTM images of each delta lobe. Delta lobes delineated by terrace scarps seen in the DEM and aerial images. For example, note the change in elevation between SL and adjacent land.

Optically-stimulated luminescence dating

Overview of OSL dating

In this study, I apply optically-stimulated luminescence (OSL) dating techniques to constrain the depositional history of the north and south delta lobes on the Goose River. OSL dating is increasingly used in fluvial deposits to determine the time elapsed since sand- and silt-sized grains were exposed to solar radiation during transport (Aitkin,

1998). After deposition and burial of sediment, grains are exposed to naturally occurring ionizing radiation (from U, Th, Rb, and K). During exposure to ionizing radiation, electrons accumulate over time in defects in the crystalline structure of (quartz and feldspar) minerals. Trapped electrons are released when exposed to light, emitting a luminescence signal. The luminescence signal (equivalent dose, D_e) is measured in the laboratory and is proportional to the deposition age. A key advantage of OSL dating over other Quaternary dating techniques, such as radiocarbon dating, is that it directly dates the depositional age of sediment and does not require *in situ* organic matter, which is often absent in fluvial systems or does not correspond with depositional age.

OSL sample collection

Sediment cores of overbank deposits from two moribund Goose River delta lobes were collected using 38 or 50 mm diameter opaque PVC pipes. Approximately 1.5 m long cores were driven into the subsurface using a dead blow mallet to minimize sediment disturbance and compaction and sealed to prevent sediment and pore water loss and avoid light exposure. A trench was dug adjacent to the sediment cores to classify grain size and interpret stratigraphic units. Additional sediment samples were collected from each OSL sample location and from four vibracore sediment cores on the active lobe for laboratory grain size analysis.

In total, 10 samples from four sediment cores were taken for OSL dating purposes (Figure 5). Overbank locations were chosen as dating sites to capture the depositional age of the delta. We selected overbank locations that were between distributary channels (i.e. mouth-bar areas) to minimize contamination from recent sediments washed into

moribund channels during floods. Individual sediment cores were subsampled into 10 cm long sections taken at various depths; the uppermost sample was chosen to determine the abandonment age (Figure 5) and a second sample was taken at depth to get sedimentation rates of each delta lobe. The uppermost sample of each core was taken from the sand-dominated layer beneath the organic-rich, rooted horizon to determine the abandonment of each lobe. The sand layer was chosen because it was formed by fluvial processes, while the organic layer may have accumulated following delta abandonment. Subsampling of core sections occurred in dark room facilities at Boston College. Subsampled sections were wrapped in plastic film and two layers of aluminum foil and covered with heavy-duty light-blocking fabric for shipping and handling (Shen et al., 2012). OSL dating took place at the University of St. Andrews, Scotland, UK using the standard SAR protocol developed by *Murray and Wintle* (2000) to obtain equivalent doses (D_e) for each sample.

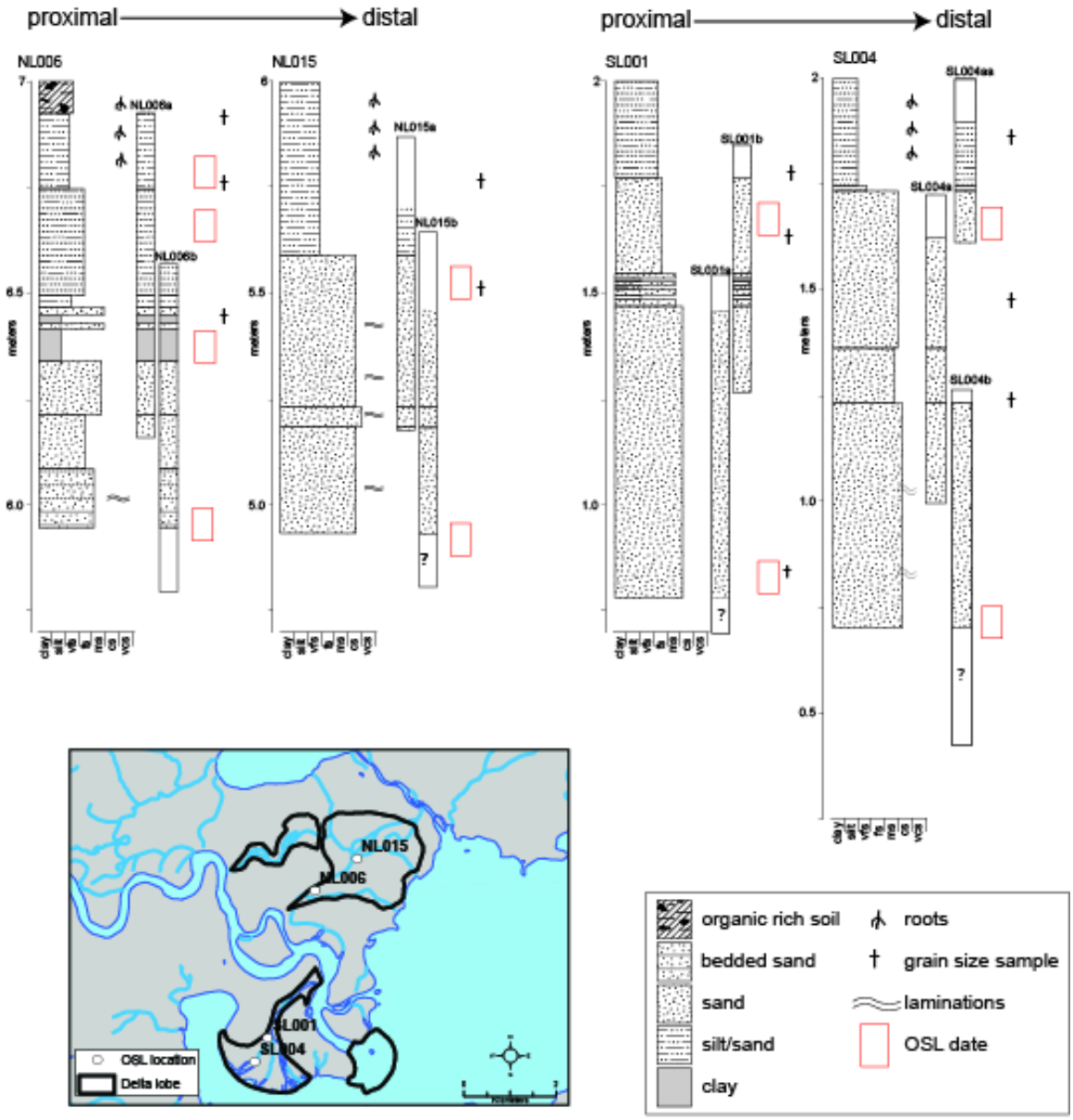

Figure 5. Stratigraphic columns showing OSL sample depths. Refer to map within the image for OSL locations. Stratigraphy was interpreted in the field from a trench adjacent to OSL cores. Grain size ranges from fine to coarse sand. OSL samples were collected from four locations, two on NL and two on SL. Multiple samples were collected at each location to determine sedimentation rates.

3.3 Results

DEM analysis

Table 1. Descriptions of each Goose River delta lobe

Delta lobe	Area (sq km)	D50 ± 1σ (μm)	Mean SRTM Elevation ± 1σ (m amsl)	Mean dGPS Elevation ± 1σ (m amsl)	RMSE (m)
NWL	0.8	-	9.0 ± 1.7	-	-
NL	3.7	260 ± 140 (n=6)	5.0 ± 1.6	5.1 ± 1.4	1.0 (n=21)
SL	1.0	220 ± 150 (n=6)	2.0 ± 1.4	2.1 ± 1.4	1.3 (n=12)
AL	1.9	370 ± 180 (n=33)	0.8 ± 0.6	0.7 ± 0.7	1.0 (n=3472)

Our analysis shows that the delta lobes were deposited at distinct elevations that are progressively lower moving from the northwest to southeast (Figures 6, 7; Table 1). The mean elevations of the abandoned lobes are 9 ± 1.7 m (NWL), 5 ± 1.6 m (NL), and 2 ± 1.4 m a.s.l (SL) and the mean elevation for the presently active lobe at the mouth of the Goose River (AL) is 0.7 ± 0.7 m a.s.l. SRTM elevation points agree with collected GPS data (Figure 8). The $RMSE_{DEM}$ for all collected elevation data points is 1.0 m and coincides with previous SRTM accuracy assessments in low-lying floodplain areas (Schumann et al., 2008). Mean GPS-derived and mean SRTM-derived elevations of NL and SL are statistically different ($p<0.05$) and differences in lobe elevations are observed in the field, providing evidence that SRTM DEM data reliably captures differences in elevations between the four measured delta lobes. To estimate the paleo-slope of the active and abandoned lobes, we computed the average elevation across radial swaths (Figure 9). The longitudinal slopes of lobes NWL and NL are $1x10^{-3}$ and $5x10^{-4}$,

respectively, while SL and AL are flat enough that a slope cannot be constrained given the errors of elevation measurement.

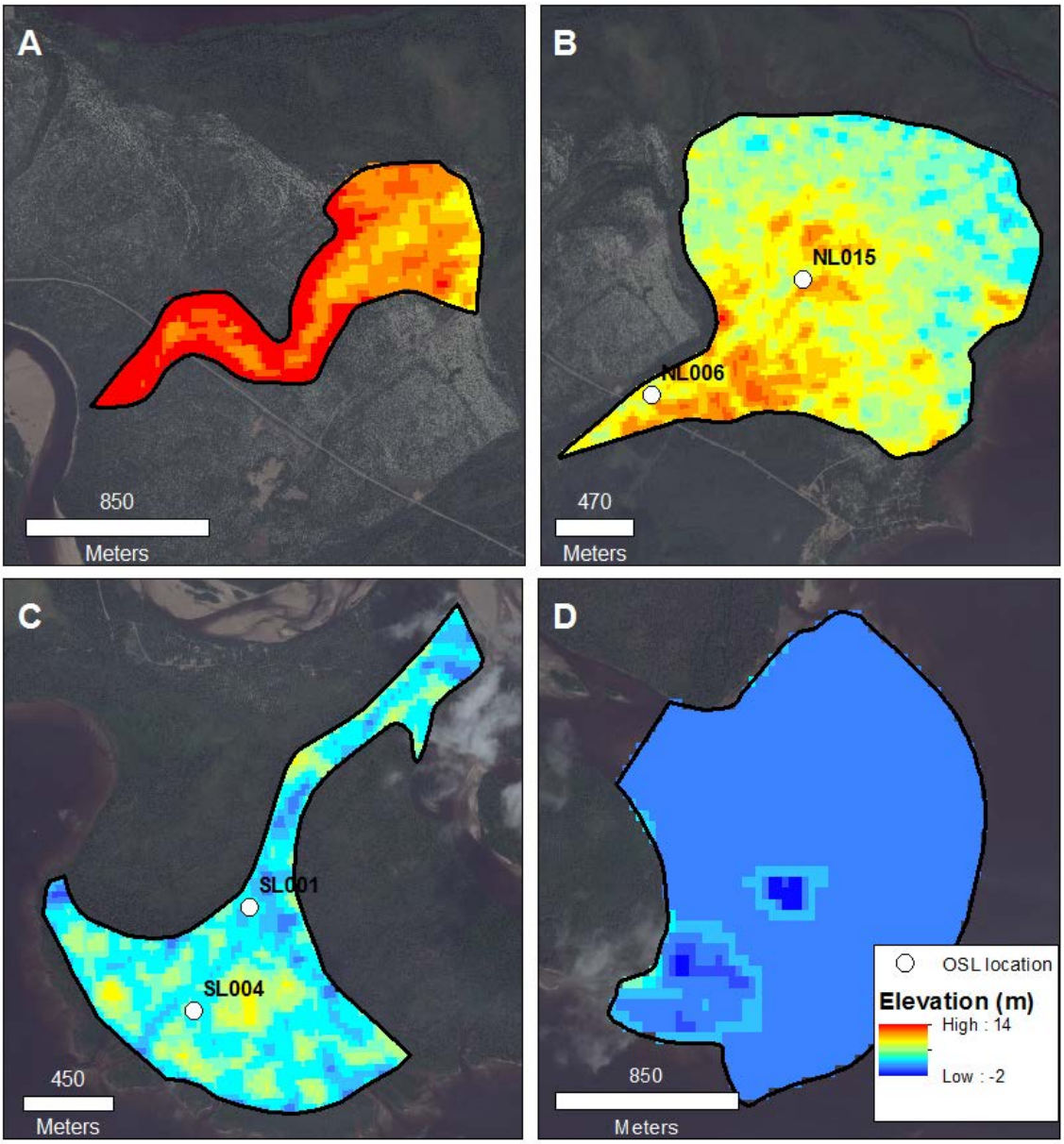

Figure 6. Detailed map showing SRTM data for Goose River delta lobes (A) NWL, (B) NL, (C) SL, and (D) AL. Deltaic land basinward of the dashed line in (C) has likely been modified by tides and/or ice and was not included in SRTM DEM analysis.

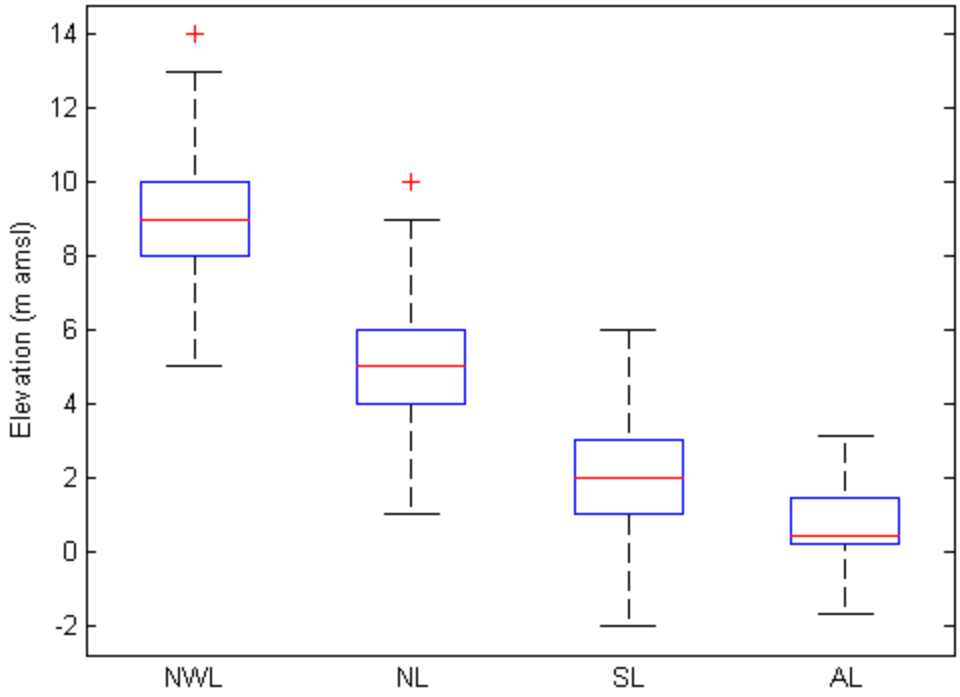

Figure 7. Boxplots showing elevation distributions of SRTM DEM data for delta lobes AL, SL, NL, and NWL. Outliers are plotted as red cross-hairs. The mean elevations of each lobe are 9 m, 5 m, 2 m, and 0.8 m a.s.l., respectively. Boxplots show that deltas were deposited at progressively lower elevations.

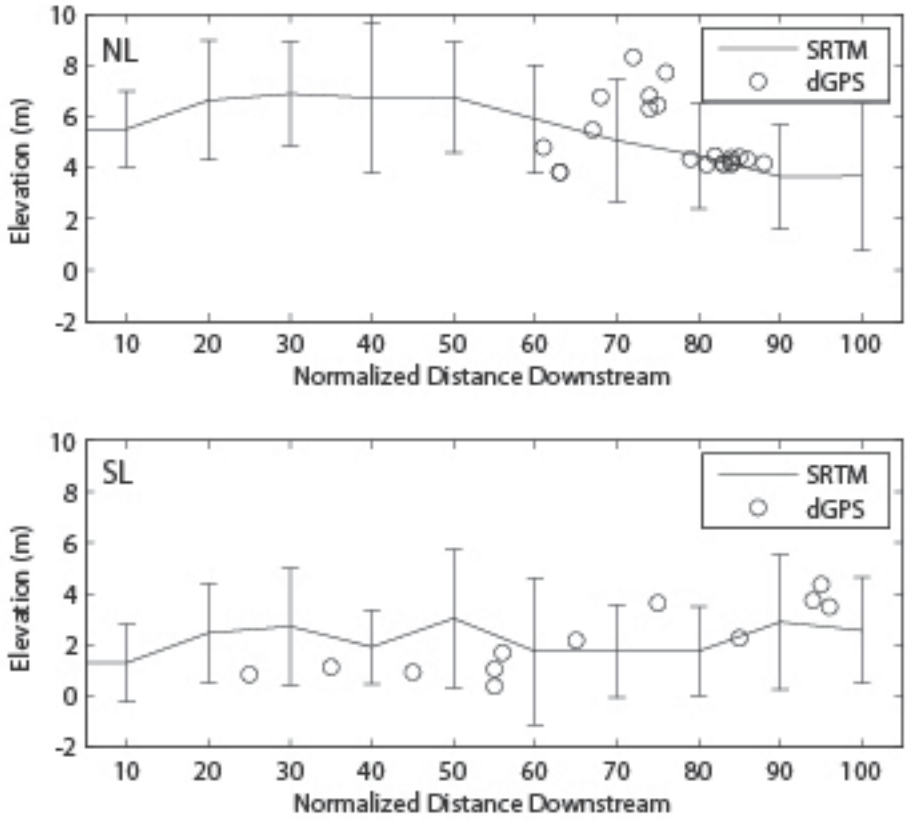

Figure 8. GPS points plotted on the radial-averaged longitudinal profile (Figure 9). Error bars are ± 2σ. GPS points generally agree with SRTM DEM data.

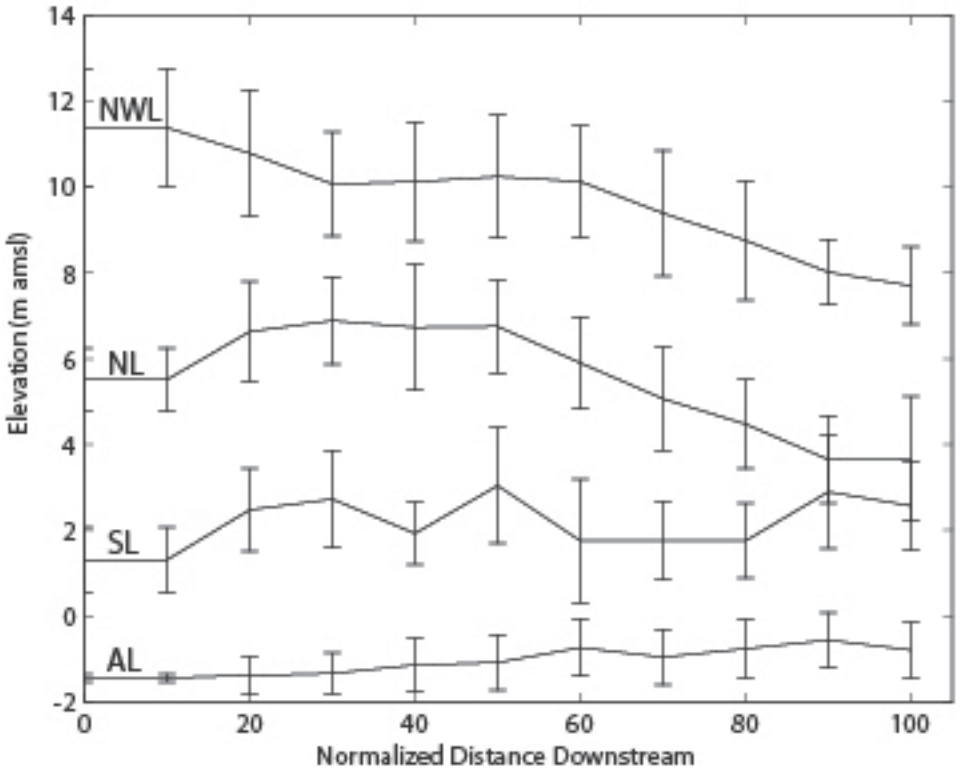

Figure 9. Radially-averaged longitudinal profiles for delta lobes AL, SL, NL, NWL. Normalized downstream distances measure the percentage of overall length. Error bars are ± 1σ for each radial swath.

We interpret the most distal part of the longitudinal profile as paleo-shoreline elevations for each lobe (i.e. the 100% distance in Figure 9). Our interpretation is based on the morphology, which is consistent with a shoreline, and also the altimetric morphology, which changes rapidly across the shoreline consistent with delta front foresets. Extracting the elevations of the shorelines provides us with the shoreline elevation close to the time of abandonment. Local paleo-shoreline maps were constructed using the elevation of each delta shoreline (Figure 10). The delta shorelines are situated at 8 m, 4 m, 2 m, and 0 m. Elevation contour lines were mapped for each shoreline. The map of local paleo-shorelines suggests that deposition was not confined to the mappable

delta lobes and could have occurred over a larger area, for instance there were more outlets to the Goose River at the 4 m contour than just the NL. The shorelines also show that the south and active lobes cut through previous deltaic sediment at a higher elevation and deposited sediment at lower elevations. This depositional hypothesis is also supported in terrace scarps seen in aerial photographs.

Figure 10. Paleo-shorelines for abandoned delta lobes. Results suggest that the shoreline was not confined to the mappable delta lobe (Figure 2), but rather occurred over a larger area. Refer to text for further information.

OSL dating

The D_e values and OSL ages for all samples are listed in Table 2. The SAR protocol produces multiple D_e measurements for a number of subsamples (aliquots) in a given sample. This technique is advantageous because it allows an internal consistency check of the sample and mitigates problems related to incomplete signal zeroing (bleaching) at the time of deposition (Rhodes, 2011). To obtain a D_e for OSL age calculation, the distributions of each sample were analyzed using two statistical approaches. For well-bleached, unimodal samples that are normally distributed the central age model (CAM) accurately characterizes the age of the distribution (Galbraith et al., 1999). For samples that are insufficiently bleached (likely containing more than one population within the sample) and have skewed distributions, the minimum age model (MAM) provides a better characterization of the age. In general, the CAM was used for samples on the northern lobe (NL) and the MAM was used on the southern lobe (SL). Geomorphic evidence suggests that there are multiple populations of grains in the SL samples; topographic scarps seen in aerial images and the DEM suggest that SL cannibalized sediment from an older terrace (Figure 4). Cannibalized sediment may be less likely to be fully bleached, justifying the use of the MAM for SL samples. Moreover, the distributions of D_e are decidedly non-normal and they did not pass any standard statistical test for normality of the distributions, further justifying the use of the MAM rather than the CAM (Figure 11).

Table 2. Equivalent Dose and OSL Age Estimates for each sample

Sample	N (aliquots)	De (Gy)	Error (Gy)	Age (ka)	Error (ka)	Age Model
NL006-01	58	5.8293	0.3524	2.0225	0.1287	MAM
NL006-02	59	6.5394	0.2346	2.5118	0.1053	CAM
NL006-03	55	7.0183	0.2872	2.6044	0.1170	CAM
NL006-04	66	5.1456	0.2774	2.0742	0.1200	CAM
NL015-01	70	3.0944	0.2978	1.2263	0.1209	CAM
NL015-03	67	5.1744	0.8802	2.1157	0.3626	MAM
SL001-01	51	2.6242	0.2323	1.0538	0.0890	MAM
SL001-03	47	3.4096	0.2155	1.3486	0.0890	MAM
SL004-02	56	2.8554	0.1841	1.1505	0.0772	MAM
SL004-04	56	4.1141	0.2282	1.7855	0.1056	MAM

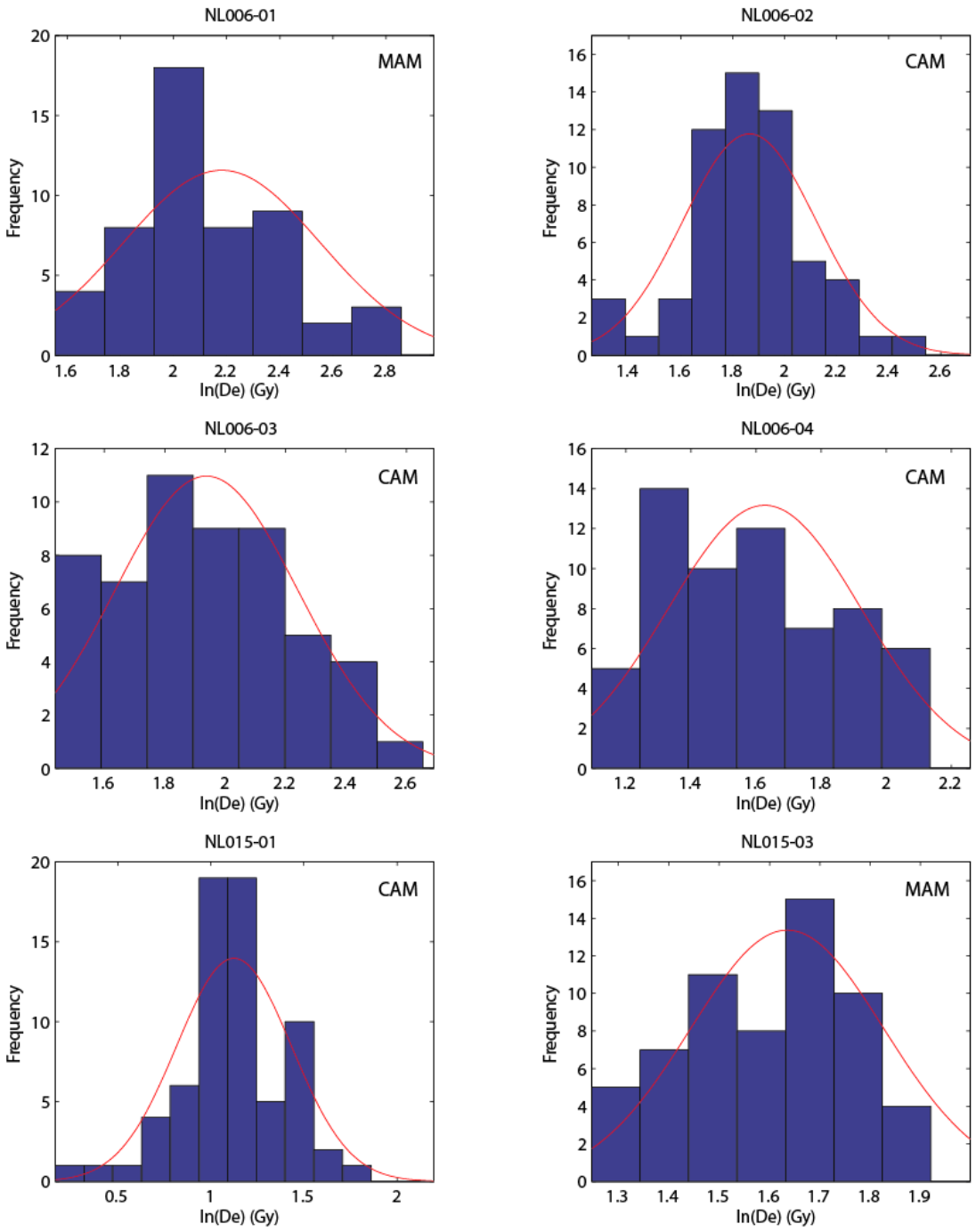
NL006-01
MAM
Frequency
ln(De) (Gy)
NL006-02
CAM
Frequency
ln(De) (Gy)
NL006-03
CAM
Frequency
ln(De) (Gy)
NL006-04
CAM
Frequency
ln(De) (Gy)
NL015-01
CAM
Frequency
ln(De) (Gy)
NL015-03
MAM
Frequency
ln(De) (Gy)

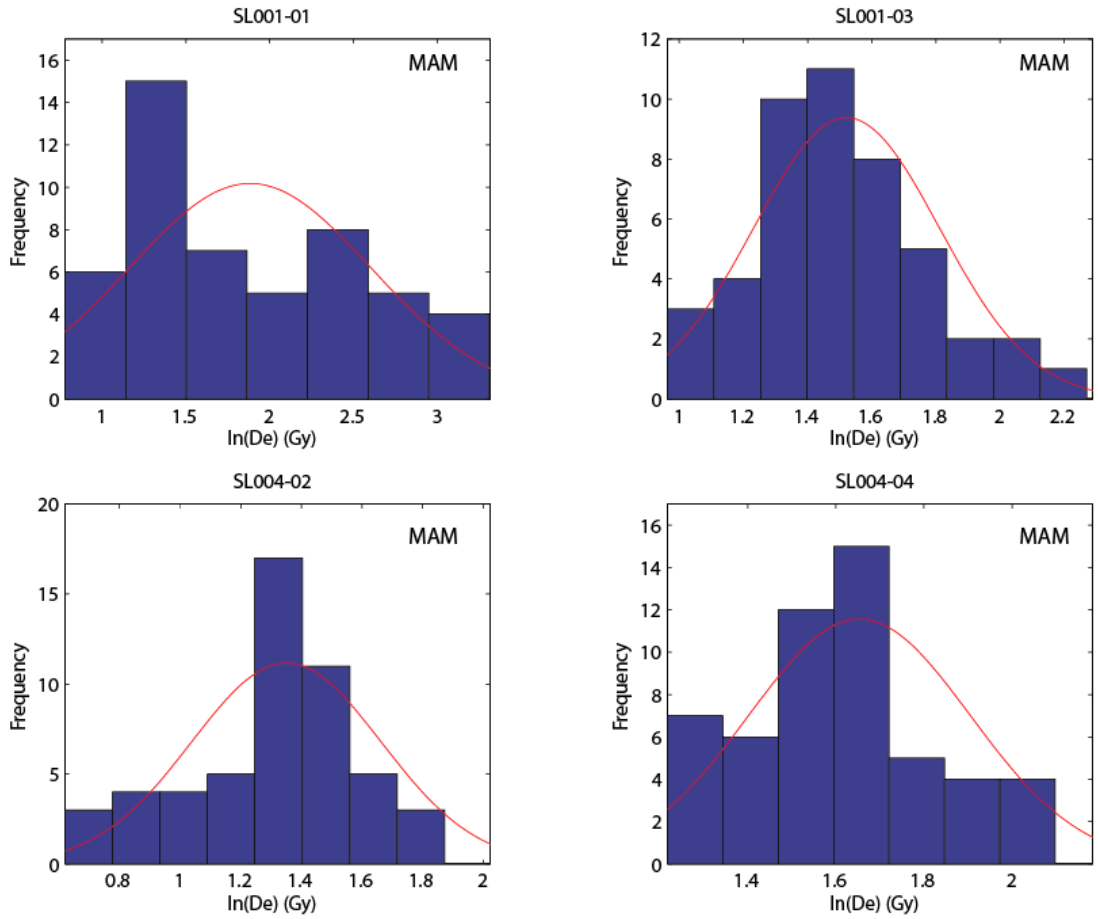

Figure 11. Histograms of D_e for OSL samples at NL and SL. Bin width is (Standard Deviation)/2. In general, NL sample distributions are unimodal and SL distributions are skewed.

Elevation data and OSL ages suggest that a series of downstepping terraced delta lobes formed at the mouth of the Goose River during a period of RSL fall. Average OSL dates are 2.1 ± 0.5 ka for NL (5 m a.s.l.) and 1.3 ± 0.3 ka for SL (2 m a.s.l.). Except for NL015-01, OSL ages on the northern lobe are older than the southern lobe (Figure 12). Sedimentation rates on the southern lobe are between 2 and 3 mm/yr. Core NL006 produced sedimentation rates of 0.3 mm/yr for the top 15 cm of the core and 4 mm/yr for the middle section of the core. The bottom date was younger than overlying deposits,

suggesting that this date is unreliable. Core NL015 produced sedimentation rates of 0.6 mm/yr.

OSL dates provide evidence that the Goose River delta switched positions from NL to the SL between 1 and 2 ka. OSL dates from NL006 show a decrease in sedimentation rate through time. This may suggest that lobe-switching was not instantaneous, but rather there was a period when both lobes received flow. Indeed, we see that previous radiocarbon samples date the abandonment of NL at 0.5 ka, which is younger than our OSL dates on SL (Newfoundland and Labrador, 2001). Further evidence for this hypothesis is seen in NL015 dates and the shoreline map. The OSL date from NL015-02 (1.23 ± 0.12 ka) is younger than SL OSL dates. NL015-02 is an uppermost sample, suggesting that the abandonment process was slow and the northern lobe may have received some flow while the southern lobe was active. Currently, we observe this with the southern and active lobe, where the southern lobe continues to receive intermittent flow.

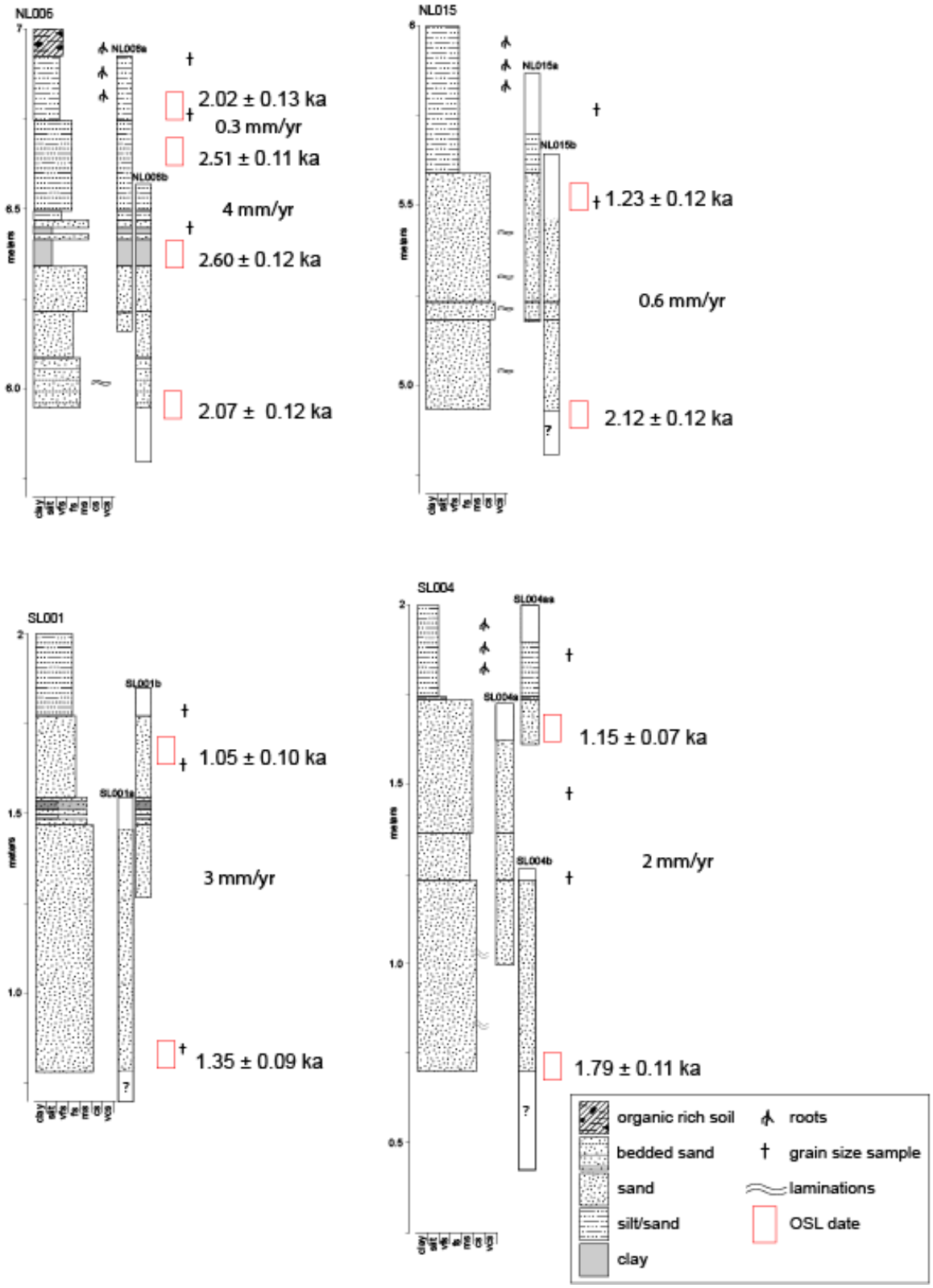

Figure 12. Stratigraphic columns with plotted OSL dates. Refer to Figures 5 or 6 for locations.

4. Numerical modeling

The field data clearly show that multiple delta lobes were constructed during a period of RSL fall. It is unclear how or why the Goose River continued to form multiple delta lobes during RSL fall, rather than incising vertically and exporting sediment offshore. To further investigate the mechanisms of delta lobe formation and avulsion during RSL fall we conducted idealized numerical modeling.

4.1 Model description

Numerical model simulations were implemented using Delft3D to isolate the fluvio-deltiac response to sea-level fall. Delft3D is a computational fluid dynamics package that simulates fluid flow, sediment transport, and morphological changes at timescales from seconds to years by solving the fluid and sediment transport and deposition equations. The hydrodynamic and morphodynamic modules are fully coupled in Delft3D, meaning the flow field adjusts to changes in bed topography in real time. The governing equations are expressed below. Further details on the application of these equations in Delft3D is described in detail by *Lesser, et al.* (2004) and the Delft3D manual (Deltares, 2011).

The purpose of this modeling study was to determine how a river such as the Goose River may evolve during sea-level fall. Our modeling approach was not to replicate exactly the Goose River and its associated deltas perfectly, but rather present a "Goose Bay-like delta" using the same general hydrologic and sedimentologic boundary conditions observed on the lower Goose River as inputs. This approach was chosen because it is impossible to precisely know the boundary and initial conditions under

which the Goose River delta lobes formed. With this model design, we can isolate the relationship between sea-level fall and delta morphology evolution and link model results with real-world data.

4.2 Governing Equations

Conservation of Momentum

Delft3D solves the three-dimensional conservation of momentum equations for unsteady, incompressible, turbulent flow to calculate the flow field. The x-,y-, and z-directed equations are

$$\left(\frac{\partial U_x}{\partial t}+U_x\frac{\partial U_x}{\partial x}+U_y\frac{\partial U_x}{\partial y}+U_z\frac{\partial U_x}{\partial z}\right)-fU_y=-\frac{1}{\rho}\left[\frac{\partial p}{\partial x}+\left(\frac{\partial \tau_{xx}}{\partial x}+\frac{\partial \tau_{yx}}{\partial y}+\frac{\partial \tau_{zx}}{\partial z}\right)\right]+g_x \quad (4.1)$$

$$\left(\frac{\partial U_y}{\partial t}+U_x\frac{\partial U_y}{\partial x}+U_y\frac{\partial U_y}{\partial y}+U_z\frac{\partial U_y}{\partial z}\right)-fU_x=-\frac{1}{\rho}\left[\frac{\partial p}{\partial y}+\left(\frac{\partial \tau_{xy}}{\partial x}+\frac{\partial \tau_{yy}}{\partial y}+\frac{\partial \tau_{zy}}{\partial z}\right)\right]+g_y \quad (4.2)$$

$$\left(\frac{\partial U_z}{\partial t}+U_x\frac{\partial U_z}{\partial x}+U_y\frac{\partial U_z}{\partial y}+U_z\frac{\partial U_z}{\partial z}\right)=-\frac{1}{\rho}\left[\frac{\partial p}{\partial y}+\left(\frac{\partial \tau_{xz}}{\partial x}+\frac{\partial \tau_{yz}}{\partial y}+\frac{\partial \tau_{zz}}{\partial z}\right)\right]+g_z \quad (4.3)$$

where U_x, U_y, U_z are the x-, y-, and z-directed fluid velocities (m/s); p is fluid pressure (N/m^2), f is the Coriolis parameter (1/s), ρ is fluid density (kg/m^3), τ is fluid shear stress (N/m^2), and g is acceleration due to gravity (m/s^2).

Conservation of fluid mass

The fluid mass balance equation, or Continuity Equation, is

$$\frac{\partial U_x}{\partial x}+\frac{\partial U_y}{\partial y}+\frac{\partial U_z}{\partial z}=0 \quad (4.4)$$

Sediment transport

Sediment transport is calculated using *van Rijn* (1993). With this approach, the sediment fraction above and below a reference height is treated as either suspended load or bedload. For simulations without waves, bedload transport is calculated as

$$|S_b| = f_{bed}\eta 0.5\rho_s D_{50} u_*' D_*^{-0.3} T \tag{4.5}$$

where $|S_b|$ is the bedload transport rate (kg/s/s), f_{bed} is a user-defined calibration factor, η is the relative availability of the sediment fraction in the mixing layer, u_*' is the effective shear velocity, D_* is the dimensionless particle diameter,

$$D_* = D_{50}\left[\frac{(s-1)g}{\nu_k{}^2}\right]^{\frac{1}{3}} \tag{4.5a}$$

where ν_k is the kinematic viscosity (m^2/s), s is density of sediment, ρ_s (kg/m^3), divided by the fluid density, ρ (kg/m^3) and T_b is the dimensionless bed-shear stress.

$$T_b = \frac{(U_*')^2 - (U_{*Cr})^2}{U_{*Cr}{}^2} \tag{4.5b}$$

where U_{*cr} is the critical shear velocity (m/s) of the median grain size and

$$U_*{}' = \left(\frac{C}{C\prime}\right)^2 U_* \tag{4.5c}$$

is the effective shear velocity where C is the overall Chezy coefficient and C' is the Chezy coefficient related to grains.

Suspended-sediment transport is calculated by solving the three-dimensional advection-diffusion equation for suspended sediment

$$\frac{\partial c^i}{\partial t} + \frac{\partial U_x c^i}{\partial x} + \frac{\partial U_y c^i}{\partial y} + \frac{\partial (w - w_s^i) c^i}{\partial z} = \frac{\partial}{\partial x}\left(\epsilon_{s,x}^i \frac{\partial c^i}{dx}\right) + \frac{\partial}{\partial y}\left(\epsilon_{s,y}^i \frac{\partial c^i}{dy}\right) + \frac{\partial}{\partial z}\left(\epsilon_{s,z}^i \frac{\partial c^i}{dz}\right) \tag{4.6}$$

where c^i is the mass concentration of the ith sediment fraction (kg/m^3), w^i_s is the hindered sediment settling velocity of the ith sediment faction (m/s) and ε represents the

sediment eddy diffusivities of the *i*th sediment fraction (m^2/s) in the horizontal (x,y) and vertical (z).

Bed-level changes

Changes in bed elevation are computed by solving the sediment continuity equation

$$\left(1-\varepsilon_{por}\right)\frac{\partial z_b}{dt}=-\frac{\partial S_x}{dx}-\frac{\partial S_y}{dy}+T_d \tag{4.7}$$

where ϵ_{por} is bed porosity, z_b is the bed level (m), S_x, S_y are the total sediment transport components per unit width in the x and y directions (m^2/s), and T_d is the deposition or erosion rate of suspended sediment (m/s).

Morphological scale factor

To enable faster computational time, a morphological scale factor of 175 was applied to at each time step. A morphological scale factor is a user-defined integer multiplying the mass deposition or erosion rate in each time step, expressed as

$$\Delta t_{morphology} = MSF \text{ x } \Delta t \tag{4.8}$$

where $\Delta t_{morphology}$ is the elapsed morphologic time, MSF is a morphologic scale factor, and Δt is the elapsed hydrodynamic time.

4.3 Model setup

The model domain consists of an elongated river channel entering into a rectangular basin (Figure 13). Computational grid cells are 25 m by 25 m. The river

channel is 150 m wide, 2 m deep, and 4,050 m long and cuts through the center of a 1150 m wide subaerial floodplain. Channel dimensions were chosen to resemble the Goose River. The initial longitudinal channel slope is 7 x 10^{-5}, which is the computed equilibrium profile. The channel enters the basin from the south through a 500 m long subaerial beach. The ocean basin is 7500 m wide and 5475 m long, with a linear basin slope of 1 x 10^{-3}. The simplified basin geometry is based on known depths of Terrington Basin (Blake Jr., 1956), though the detailed bathymetry during delta formation is unknown. A 0.05 m white-noise model was applied to the grid to simulate natural variations in bathymetry. A uniform bed roughness is set to a spatially and temporally constant Chezy value of 45 $m^{1/2}/s$ and an initial 10 m of erodible sediment is available throughout the domain.

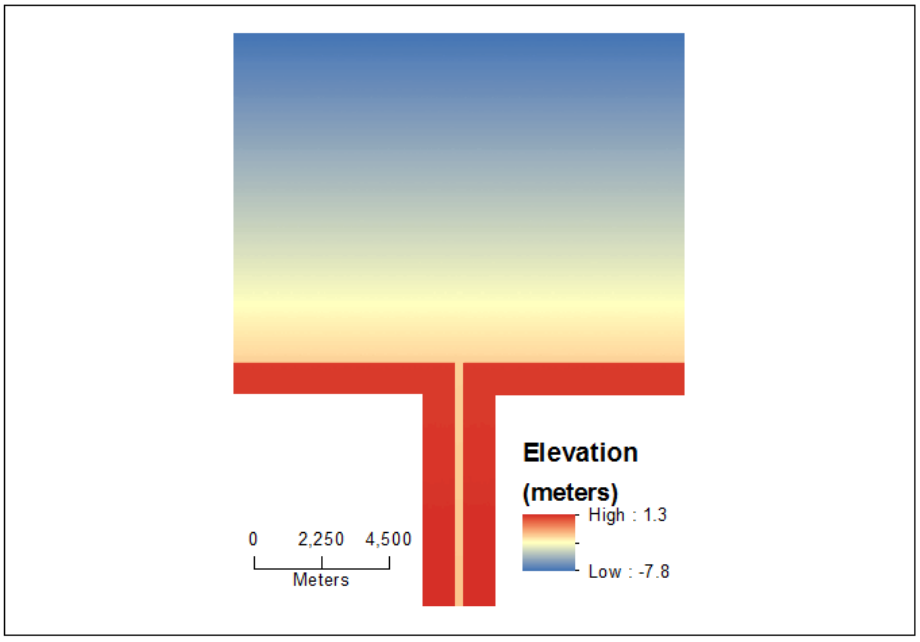

Figure 13. Domain and initial bathymetry for Delft3D models.

Water supply and RSL are prescribed at the southern and northern boundaries. A spatially and temporally invariant water discharge of 300 m^3/s and equilibrium sediment concentration enters the river channel from the southern (bottom) border. Sediment entering the system and available on the bed has a single grain size of 350 µm, which is the median grain size of the active Goose River delta lobe. A temporally variable water surface elevation (sea-level) is set at the northern (top) boundary.

Before the onset of sea-level fall, a 0.9 km^2 delta with associated channels and bars (Figure 14) was allowed to prograde basinward over a 150-year morphological period, until the delta topset slope reached a dynamic equilibrium. The establishment scenario was implemented to isolate initial delta growth from sea-level fall. The bathymetry following the 150-year morphologic period was used as the starting point for each model under varying sea-level.

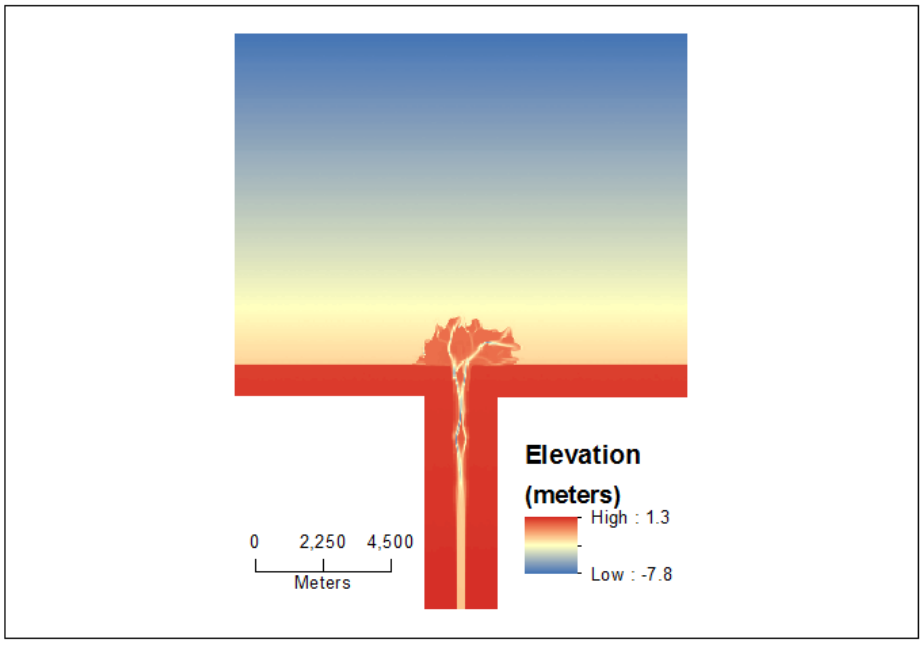

Figure 14. Establishment scenario bathymetry.

RSL fall simulations

Table 3. Delft3D Model parameters

User-defined Model Parameter	**Value**	**Units**
Cell size	25 x 25	m
Initial basin bed slope	$1x10^{-3}$	-
Initial channel bed slope	$7x10^{-5}$	-
Initial channel dimensions (width x depth)	150 x 2.0	m
Initial sediment layer thickness at bed	10	m
Sediment grain size	350	μm
Time step	0.2	min.
Chézy value	45	$m^{1/2}/s$
Background horizontal eddy viscosity and diffusivity	$1x10^{-4}$	m^2/s
Morphological scale factor	175	-
Downstream open boundary (sea-level)	See Table 3	-

We ran 11 modeling scenarios with sea-level fall rates ranging between 0 and 10 mm/yr. Model parameters and RSL fall scenarios are shown in Tables 3 and 4. This was done to capture the range of possible RSL fall rates of Goose Bay over the past 2000 years (Clark and Fitzhugh, 1993; Blake Jr., 1956). In Delft3D the use of a morphological scale factor speeds up the morphological time scale relative to the hydrodynamic time scale. To simulate the morphologic changes under a given sea-level fall rate, the hydrologic boundary conditions must also be scaled by the morphologic scale factor, as follows

$$\frac{dRSL/dt \cdot \Delta t \cdot MSF}{I} = \Delta E \quad (4.9)$$

where dRSL/dt is the relatively sea-level fall rate (m/yr), Δt is the elapsed time in the model run (years),

I is a flow intermittency factor, and ΔE is the change in water surface elevation (m) implemented in Delft3D at the downstream boundaries. We introduced *I* into the equation because the simulations have a constant discharge, which means the delta channels are at bankfull discharge continuously during the simulation. By eliminating the low-flow portion of the hydrograph we effectively speed up our simulations. To accurately model a given *S*, we must take into account this intermittency. As a starting point we assume that bankfull discharge occurs over a period of 14 days every year, and we set $I = 0.038$, which is the fraction of days per year a river is at bankfull discharge. This allows us to scale ΔE according to how much geomorphic time elapsed in the simulation.

Table 4. Sea-level fall scenarios

Run ID	Sea-level rate (mm/yr)
A1_0mm	0
A1_1mm	-1
A1_2mm	-2
A1_3mm	-3
A1_4mm	-4
A1_5mm	-5
A1_6mm	-6
A1_7mm	-7
A1_8mm	-8
A1_9mm	-9
A1_10mm	-10

4.4 Delft3D model results

A representative model run (RSL fall of 3 mm/yr) of the general geomorphic processes occurring during RSL fall is shown in Figure 15. Initially, a delta progrades basinward with constant RSL (Figure 15.A). After this point, sea-level was lowered at a linear rate for 300 morphological years. Flow is initially routed to the dominant channel and deposition is concentrated at the mouth of the river, resulting in a new delta lobe positioned at a lower elevation, leaving the older delta lobe terraced at a higher elevation (Figure 15.B). New delta lobes are marked after an avulsion occurs, and are recognized

because a topographic scarp separates the new lobe from the old lobe (note the higher elevation surface upstream of lobe 1 in Figure 15.B). In some instances, the topographic scarps are subtle, and lobes are delineated by observing lobe-switching in animations of delta runs. As this process continues, there are multiple terraced delta lobes at distinct elevations (Figure 15.C and 16). In some cases, multiple channels can be simultaneously active, resulting in isolated and active delta lobes (Figure 15.D).

It is interesting that during RSL fall the delta responds by creating multiple delta lobes at different elevation. We observe the activity of localized deposition and lateral migration through avulsion and lobe-switching for RSL fall rates between 1 and 10 mm/yr. Channel incision is relatively limited, with some cannibalization of previous delta deposits. The resulting planform morphology at the completion of the model run is a series of delta lobes deposited at progressively lower elevations (Figure 16).

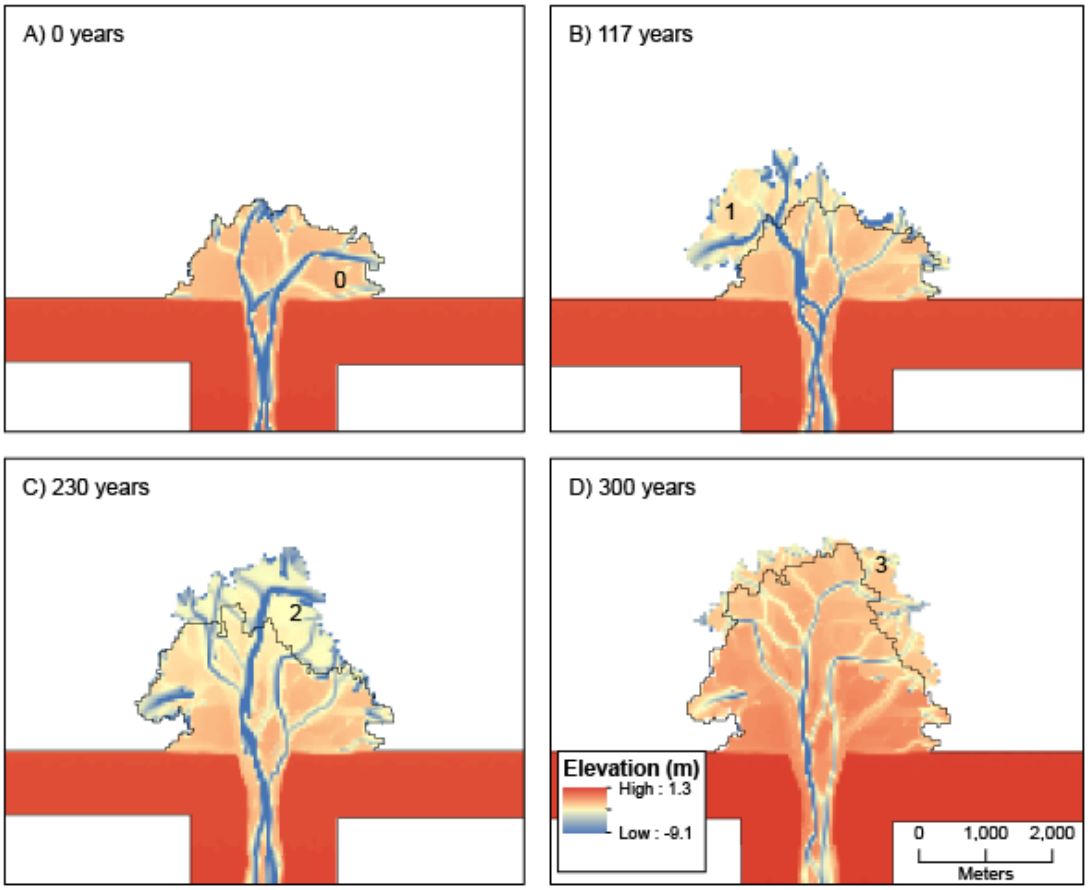

Figure 15. Delta evolution for Delft3D model run experiencing a 3 mm/yr RSL fall. Solid delta outlines represent the delta at the previous time iteration. (A) An initial delta progrades basinward with no RSL fall. After the delta reaches an equilibrium profile, sea-level begins to fall. (B) Flow is concentrated into a dominant branch, forming a new delta lobe. After 117 years, the delta avulses to a new position on the shelf. (C) The delta has migrated laterally, forming a new delta lobe that occupies a topographic low. Some sediment from the previously active delta lobes has been cannibalized at deposited on the active delta lobe. (D) Deposition continues to occur at the mouths of active channels. This may result in the contemporaneous formation of multiple isolated delta lobes.

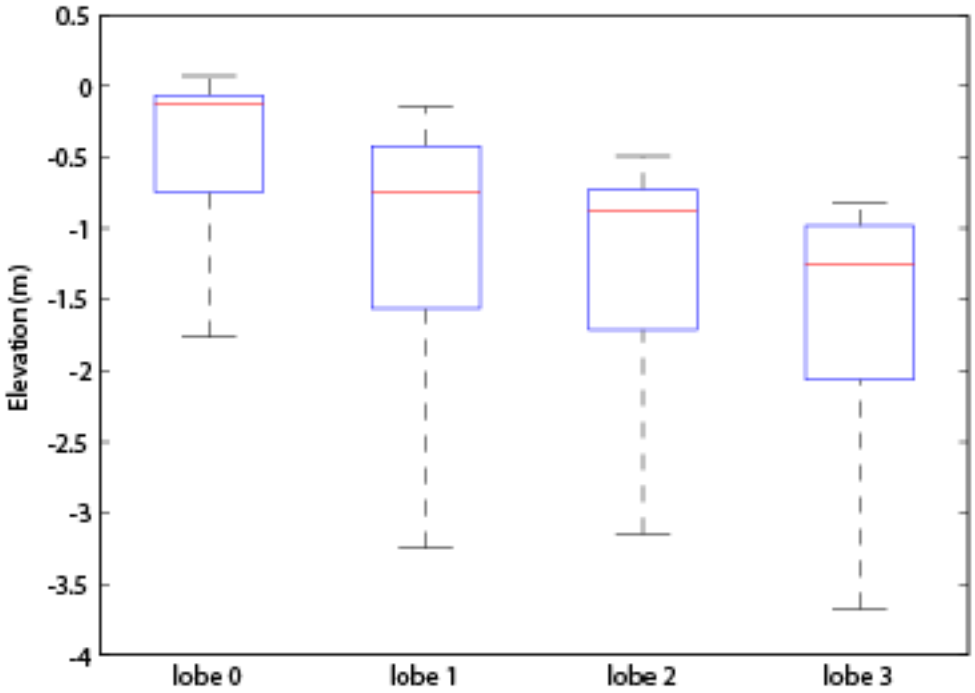

Figure 16. Boxplots showing the elevation distribution of each delta lobe formed during a RSL fall of 3 mm/yr (Refer to Figure 15).

In terms of avulsion dynamics, we noticed two important trends in our simulations (Figure 17). First, the frequency of avulsions increases with increasing RSL fall rate (Figure 18). At high RSL fall rates, avulsions occur frequently because the superelevation rate is highest. After all at high RSL fall rates, deltas prograde faster (compare Figure 17.B and D), thereby increasing aggradation rate, and the shoreline recedes fastest exposing steeper slopes. The result is a series of many, short-lived delta lobes that radially migrate across the basin and are deposited at less distinct elevations. Second, we observe that the average delta lobe width decreases with increasing RSL fall (Figure 19). Average delta lobe width decreases from 7000 m to 350 m as the sea-level fall rate increases from 0 mm/yr to 10 mm/yr.

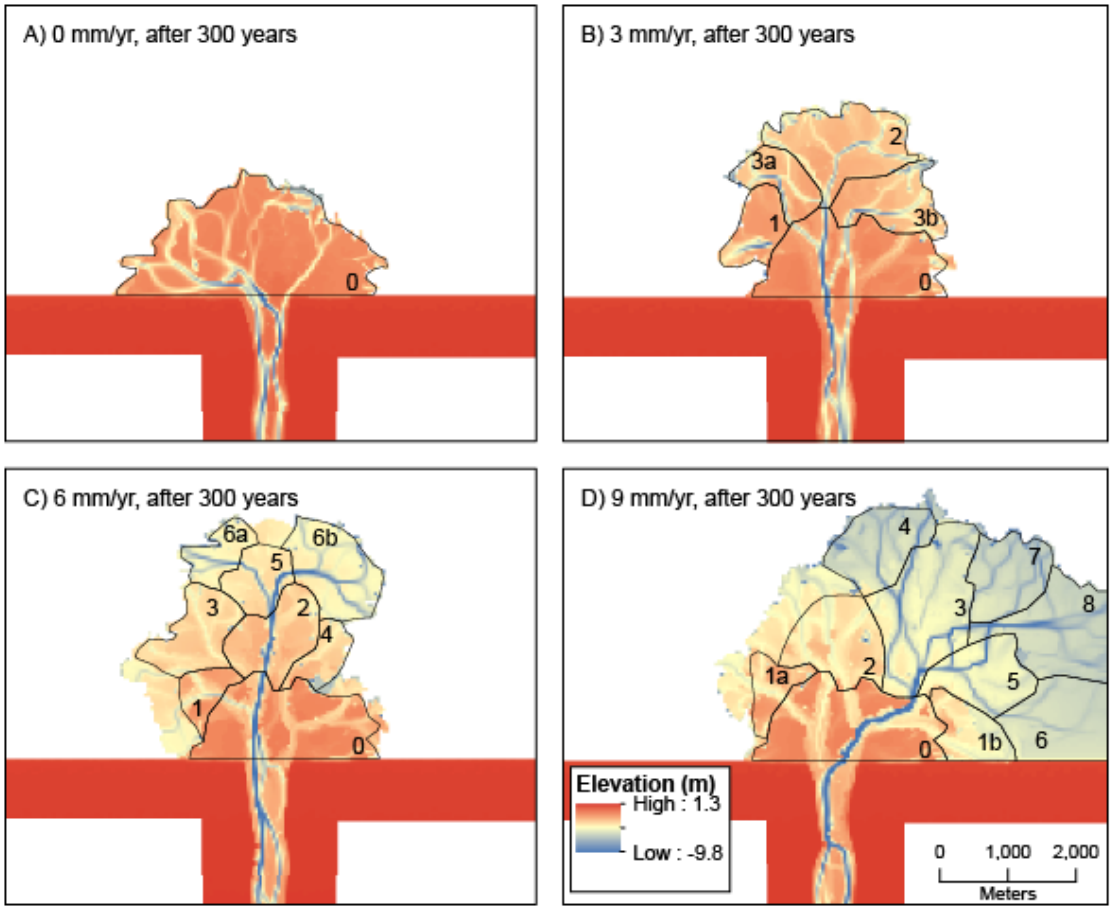

Figure 17. Planform view and elevation of Delft3D model runs after 300 years undergoing (A) 0 mm/yr, (B) 3 mm/yr, (C) 6 mm/yr, and (D) 9 mm/yr of sea-level fall. Delta lobes are numbered in chronological order of formation. In instances where multiple lobes are active, number and letter nomenclature is used. Delta lobes are hand delineated based on topographic scarps and observations from delta evolution animations.

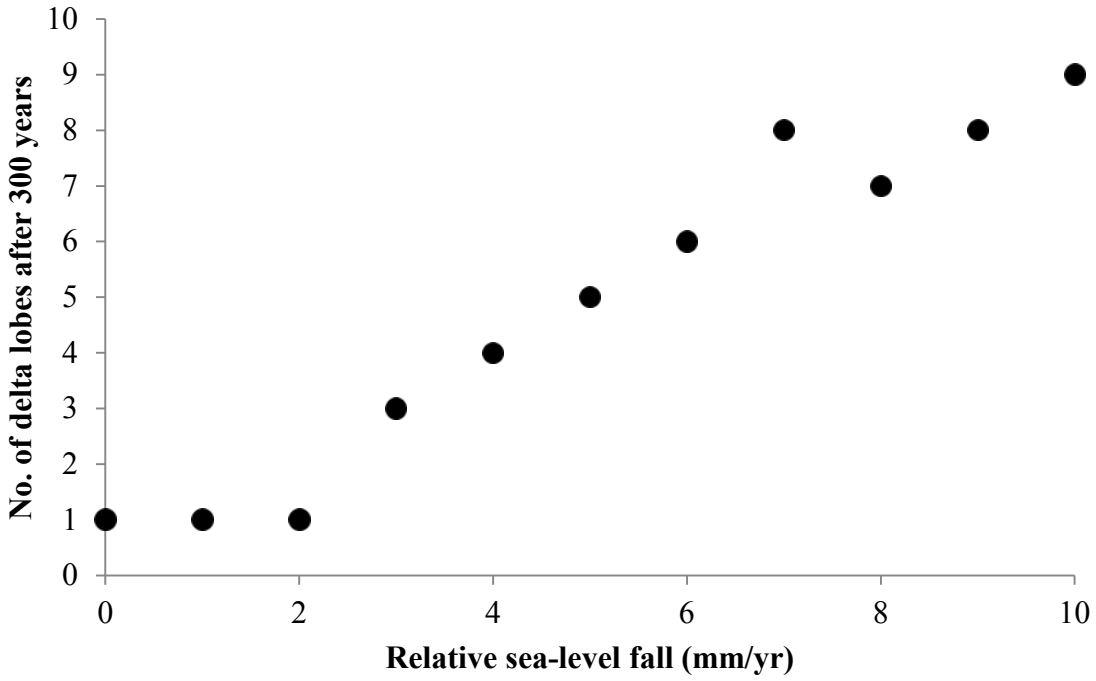

Figure 18. Plot of number of delta lobes forming after 300 model years vs. RSL fall rate.

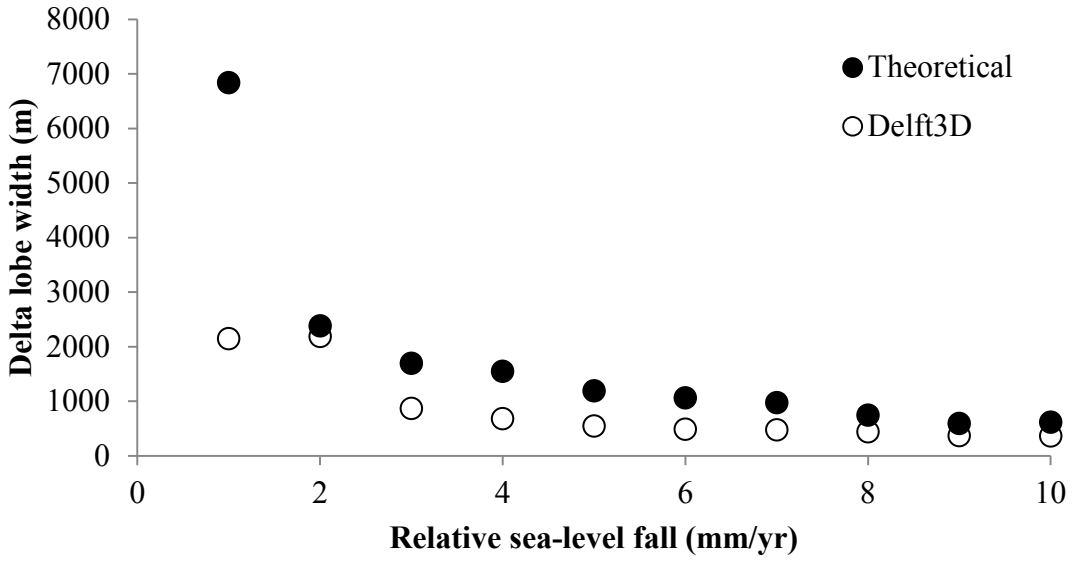

Figure 19. Plot of delta lobe width vs. RSL fall rate. Dark circles are theoretical maximum delta lobe width to remain aggradational (calculated from Eq. 6.2). Outlined circles are widths measured on Delft3D model runs.

5. Discussion

5.1 Goose Bay and comparison to Delft3D model runs

The Goose River delta formed multiple terraced delta lobes during a period of RSL fall. Similarly, Our Delft3D model runs show the formation of multiple delta lobes forming at progressively lower elevations. While Delft3D models presented here were simplified, the formation of multiple delta lobes through avulsions was observed during modeled rates of RSL fall. In our models, we only changed the rate of RSL fall and held other variables that can affect the fluvial evolution to relative sea-level fall (sediment and water supply, basin physiography) constant. Model runs suggest that the lateral migration of the Goose River delta can be explained by falling RSL, alone. Degradation was largely absent during model runs, with only some cannibalization of stranded delta lobe terraces. Observations from the field and model runs provide a critical link in understanding the geomorphic processes occurring during RSL fall, and in particular show that 1) incision and sediment bypass is not a necessary response to RSL fall and 2) lateral migration of a delta via avulsion can continue with falling sea-level.

5.2 Aggradation and lateral migration

Why do the Goose River and the modeled deltas continue to construct delta lobes during RSL fall rather than incising though the initial lobe and exporting sediment offshore? To understand this, we start with the observation that the width of a delta lobe scales with RSL fall rate (Figure 19**)**. This implies that delta lobes deposit sediment over a smaller area in response to an increase in RSL fall rate. By forming smaller delta lobes, a fluvio-deltaic system may remain aggradational, leading to conditions favorable for

avulsion. This idea is supported computationally through geometric analysis and diffusion modeling by *Swenson and Muto* (2007). The authors show that in principle, the aggradational phase during RSL fall can be long lived. The authors show using a scaling analysis that if the intrinsic fluvio-deltaic response time τ is longer than the periodicity of relative sea-level fall (T) (ie. $\tau > T$) then aggradation will continue to occur:

$$\tau = \frac{q_s^2}{\upsilon_f}\left|\frac{dRSL}{dt}\right|^{-2} \quad (6.1)$$

where q_s is the sediment supply per unit delta width, dRSL/dt is the rate of RSL fall, and υ_f is the fluvial diffusivity, which can be represented as kq_w where k is a constant and q_w is the water supply per unit delta width. To determine k we conducted separate experiments to find an empirical relationship between sand flux, water flux and bed slope (Figure 20) (e.g., *Swenson and Muto* (2007) and *Parker and* Muto (2003)).

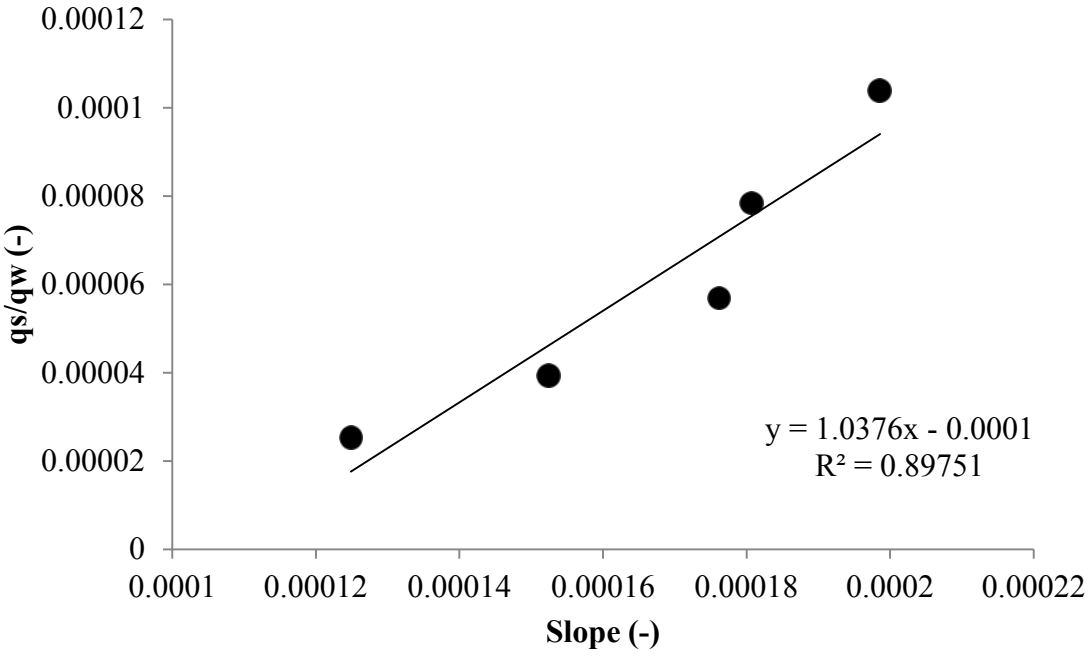

Figure 20. Empirical relationship between sediment flux, water flux, and bed lobe in Delft3D experiments. Dark circles are data from model runs. Solid line is the regression line. Y-axis represents the ratio between sediment and water flux per unit width.

In our model runs the deltas remain aggradational implying that $\tau > T$. We suggest that each delta lobe decreases its width (i.e. increases q_s in equation 6.1) to offset the increase in RSL fall and maintain $\tau > T$. By rearranging Equation 6.1 and substituting $q_s = Q_s/B$ and $\upsilon = kQ_w/B$, where Q_s and Q_w are the volumetric water sediment flux for the delta lobe and B is the average delta lobe width, it is possible to solve for the theoretical delta width required to maintain aggradation:

$$B = \frac{Q_s^2}{kQ_w T_{rsl} \left|\frac{dRSL}{dt}\right|^2} \quad (6.2).$$

We plot the theoretical and measured delta lobe widths calculated for each model run using equation 6.2 in Figure 18**.** The delta lobe width is measured as the width of the delta prior to its first avulsion following RSL fall (ex. Figure 13.B, lobe 1). The width prior to the first avulsion was measured because the majority of sediment and water supply is concentrated at this one lobe. In later stages, multiple isolated delta lobes can form at the same time, resulting in unevenly distributed sediment and water supplies. Values for sediment and water supply are measured at the upstream boundary and represent the supply entering the system. The periodicity (T_{rsl}) is measured as the time elapsed between the onset of RSL fall and the first avulsion. The theoretical width is a maximum width to remain aggradational, and we expect measured delta lobe widths to be smaller. Equation 6.2 predicts that to remain aggradational during RSL fall, delta lobe width must decrease, as seen in both observed and theoretical measurements.

Avulsions are thought to occur due to aggradation and superelevation of a channel above the floodplain (Slingerland and Smith, 2004). By remaining aggradational, lateral migration of a delta lobe through avulsions can remain possible during RSL fall.

Boxplots show the distributions of elevation for each delta lobe at the time of avulsion compared to RSL (Figure 21). I see that some of the delta lobe is deposited above sea-level, creating the superelevation criteria required for avulsion. Further, deposition is localized at the channel mouth, leading to channel extension and lowering of the longitudinal slope. Lateral deposition adjacent to the extending channel is minimal. Spatial nonuniformity in deposition leads to an advantageous cross-valley slope relative to the longitudinal slope. Following overbank flow, avulsions may be explained by superelevation and cross-valley slope advantages.

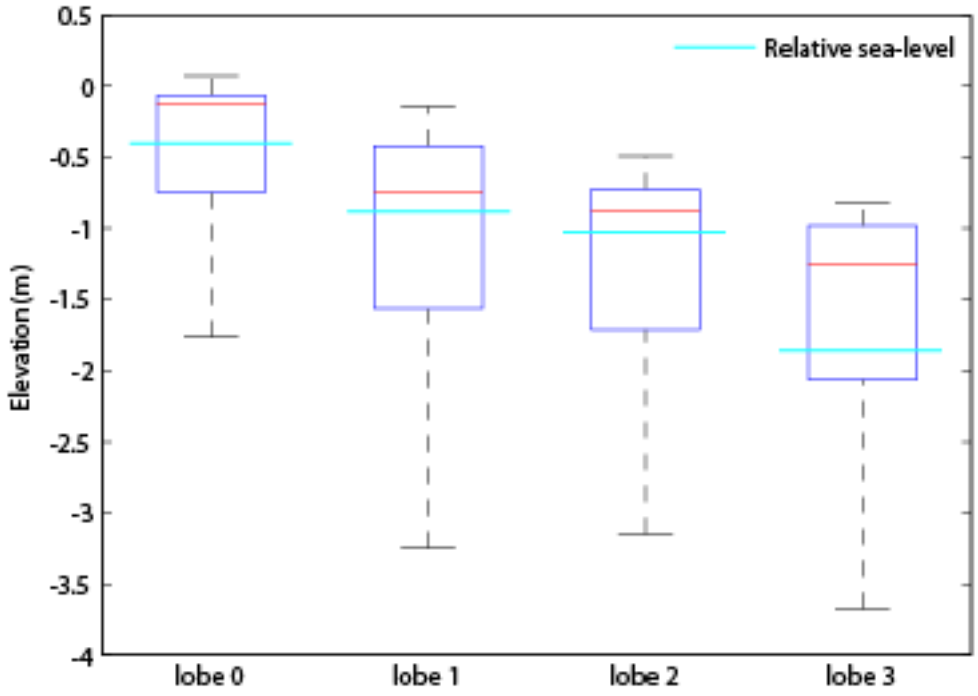

Figure 21. Boxplots of elevations for lobes associated with a 3 mm/yr RSL fall relative to sea-level conditions. Boxplots show that much of the delta was located above the regressing shoreline, potentially creating superelevation conditions favorable for avulsion.

‘Autoincision,’ or the inevitability of a fluvio-deltaic system to transition from an aggradational to degradational regime during RSL fall, is thought to be an autogenic response to steady forcing by constant sea-level fall (Muto and Steel, 2004); however, I do not observe this response in our model runs. Instead of degradation, model runs show continuous avulsions, implying continued aggradation. Avulsions may play an important role in preventing the system from attaining an autoincision threshold. Diffusion modeling demonstrates that there is an inherent time-lag between a change in RSL fall and fluvio-deltaic response caused by an upstream migrating knickpoint (Leeder and Stewart, 1996; van Heijst and Postma, 2001). The process of knickpoint migration must restart following each avulsion, effectively neutralizing the effects of relative sea-level fall. I propose that as long as the avulsion period is less than the system response to knickpoint migration, aggradation can continue to occur on the fluvio-deltaic system.

7. Conclusions

The fluvio-deltaic response to RSL fall has received considerable attention in the past; however, without modern field evidence, past models can not be verified. Here I have shown through observations of the Goose River delta and supporting Delft3D models that avulsions can continue during RSL fall. The Goose River delta has switched positions multiple times, resulting in the formation of at least four distinct delta lobes deposited at different elevations. OSL dates show that these delta lobes are temporally distinct. Modeling results that investigate the fluvio-deltaic response to RSL fall show similar planform morphologies to the Goose River delta. Model runs show continued avulsions and formation of multiple terraced delta lobes deposited at progressively lower elevations. I show computationally that by decreasing delta lobe widths, deltas may remain aggradational during RSL fall, creating conditions favorable for avulsions and deltaic lobe-switching during RSL fall. Aggradation of a delta may continue as long as the avulsion period is less than the system response time to RSL fall. Our results suggest that degradation is not a necessary response to RSL fall and that lateral migration of a delta through avulsions and lobe-switching can continue to occur with a falling sea-level.

Notation

E_{GPS}	GPS-derived elevation, m;
E_{SRTM}	SRTM-derived elevation, m;
$RMSE_{DEM}$	root mean square error between SRTM and GPS-derived elevations, m;
U_x, U_y, U_z	x-, y-, and z-directed fluid velocities, m/s;
p	fluid pressure, N/m^2;
f	Coriolis parameter 1/s;
ρ_w	fluid density kg/m^3,
τ	fluid shear stress, N/m^2;
g	acceleration due to gravity m/s^2;
$\|S_b\|$	bedload transport rate, kg/s/s;
f_{bed}	user-defined calibration factor, dimensionless;
η	relative availability of the sediment fraction in the mixing layer, dimensionless;
u_*'	effective bed shear velocity, m/s;
D_*	dimensionless particle diameter, dimensionless;
ν_k	kinematic viscosity, m^2/s;
T_b	dimensionless bed-shear stress, dimensionless;
U_{*cr}	critical shear velocity of the median grain size, m/s;
C	overall Chezy coefficient, $m^{1/2}/s$;
C'	Chezy coefficient related to grains, $m^{1/2}/s$;
c^i	mass concentration of the *i*th sediment fraction, kg/m^3;
w^i_s	hindered sediment settling velocity of the *i*th sediment faction, m/s;
ε	the sediment eddy diffusivities of the *i*th sediment fraction, m^2/s;
ϵ_{por}	bed porosity, dimensionless;
z_b	bed level, m;
S_x, S_y	total sediment transport components per unit width in the x and y directions; m^2/s;
T_d	deposition or erosion rate of suspended sediment, m/s;
$\Delta t_{morphology}$	elapsed morphologic time, years;
MSF	morphologic scale factor, dimensionless;
Δt	elapsed hydrodynamic time, years;
$dRSL/dt$	rate of RSL fall, mm/yr;
Δt	elapsed time in the model run, years;
I	flow intermittency factor;
ΔE	change in water surface elevation, m;
q_s	sediment supply per unit delta width, m^2/s;
υ_f	fluvial diffusivity
q_w	water supply per unit delta width, m^2/s;
k	constant, dimensionless;
τ	system response time, years;
T_{rsl}	periodicity of relative sea-level fall, years;
Q_s	volumetric sediment flux for the delta lobe, m^3/s;
Q_w	volumetric water flux for the delta lobe, m^3/s;

B average delta lobe width, m;

REFERENCES

Aitken, M. J. (1998). *An introduction to optical dating: the dating of Quaternary sediments by the use of photon-stimulated luminescence*. Oxford University Press.

Berry, P. A. M., Garlick, J. D., & Smith, R. G. (2007). Near-global validation of the SRTM DEM using satellite radar altimetry. *Remote Sensing of Environment*, *106*(1), 17-27.

Blake Jr, W. (1955). Note on the Dating of Terraces in the Lake Melville District, Labrador. *Science (New York, NY)*, *121*(3134), 112.

Blake Jr, W. (1956). Landforms and topography of the Lake Melville area, Labrador, Newfoundland. *Geography Bullettin, Department of Mines and Technical Survey, Ottawa, Canada*, *9*, 93-97.

Blum, M. D., & Törnqvist, T. E. (2000). Fluvial responses to climate and sea-level change: a review and look forward. *Sedimentology*, *47*(s1), 2-48.

Clark, P. U., & Fitzhugh, W. W. (1992). Coast and Interpretation of the Archaeological Record. *Paleoshorelines and prehistory: An investigation of method*, 189.

Coachman, L. K. (1953). River flow and winter hydrographic structure of the Hamilton Inlet-Lake Melville Estuary of Labrador: Blue Dolphin Labrado Expedition, unpublished manuscript. 19 p.

Deltares (2011). Delft3D-Flow Manual 3.15.566, 672 pp., Delft, Netherlands

Fairbanks, R. G. (1989). A 17, 000-year glacio-eustatic sea-level record: influence of glacial melting rates on the Younger Dryas event and deep-ocean circulation. *Nature*, *342*(6250), 637-642.

Farr, T. G., Rosen, P. A., Caro, E., Crippen, R., Duren, R., Hensley, S., & Alsdorf, D. (2007). The shuttle radar topography mission. *Reviews of geophysics*, *45*(2).

Fisk, H. N. (1944). *Geological investigation of the alluvial valley of the lower Mississippi River* (p. 78). War Department, Corps of Engineers.

Fitzhugh, W. (1973). Environmental Approaches to the Prehistory of the North. *J. Wash. Acad. Sci*, *63*(2), 40.

Galbraith, R. F., Roberts, R. G., Laslett, G. M., Yoshida, H., & Olley, J. M. (1999). Optical dating of single and multiple grains of quartz from jinmium rock shelter, northern australia: part i, experimental design and statistical models. *Archaeometry*, *41*(2), 339-364.

Henton, J. A., Craymer, M. R., Dragert, H., Mazzotti, S., Ferland, R., & Forbes, D. L. (2006). Crustal motion and deformation monitoring of the Canadian landmass. *Geomatica*, *60*(2), 173-191.

Jerolmack, D. J., & Paola, C. (2007). Complexity in a cellular model of river avulsion. *Geomorphology*, *91*(3), 259-270.

Jones, L. S., & Schumm, S. A. (2009). Causes of avulsion: an overview. *Fluvial Sedimentology VI*, 171-178.

Koss, J. E., Ethridge, F. G., & Schumm, S. A. (1994). An experimental study of the effects of base-level change on fluvial, coastal plain and shelf systems.*Journal of Sedimentary Research*, *64*(2b), 90-98.

Lane, E. W. The importance of fluvial morphology in hydraulic engineering. *Proceedings of the American Society of Civil Engineering* **81**, paper 745, 1–17 (1955). (fix)

Leeder, M. R., & Stewart, M. D. (1996). Fluvial incision and sequence stratigraphy: alluvial responses to relative sea-level fall and their detection in the geological record. *Geological Society, London, Special Publications*, *103*(1), 25-39.

Lesser, G. R., Roelvink, J. A., Van Kester, J. A. T. M., & Stelling, G. S. (2004). Development and validation of a three-dimensional morphological model.*Coastal engineering*, *51*(8), 883-915.

Liverman, D. G. (1997). Quaternary Geology of the Goose Bay Area. *Current Research. Newfoundland and Labrador Department of Mines and Energy, Geological Survey, Report*, 97-1

Mackin, J. H. (1948). Concept of the graded river. *Geological Society of America Bulletin*, *59*(5), 463-512.

Meijer, X. D. (2002). Modelling the drainage evolution of a river–shelf system forced by Quaternary glacio-eustasy. *Basin Research*, *14*(3), 361-377.

Murray, A. S., & Wintle, A. G. (2000). Luminescence dating of quartz using an improved single-aliquot regenerative-dose protocol. *Radiation measurements*,*32*(1), 57-73.

Muto, T., & Steel, R. J. (2004). Autogenic response of fluvial deltas to steady sea-level fall: Implications from flume-tank experiments. *Geology*, *32*(5), 401-404.

Paola, C. (2000). Quantitative models of sedimentary basin filling. *Sedimentology,* 47(s1), 121-178.

Parker, G., & Muto, T. (2003). 1D numerical model of delta response to rising sea-level. In *Proceedings of the Third IAHR Symposium, River, Coastal and Estuarine Morphodynamics.* (pp. 558-570).

Posamentier, H. W., Jervey, M. T., & Vail, P. R. (1988). Eustatic controls on clastic deposition I—conceptual framework. *Sea-Level Changes: An Integrated Approach: SEPM, Special Publication*, *42*, 109-124.

Rhodes, E. J. (2011). Optically stimulated luminescence dating of sediments over the past 200,000 years. *Annual Review of Earth and Planetary Sciences*,*39*, 461-488.

Schumann, G., Matgen, P., Cutler, M. E. J., Black, A., Hoffmann, L., & Pfister, L. (2008). Comparison of remotely sensed water stages from LiDAR, topographic contours and SRTM. *ISPRS Journal of Photogrammetry and Remote Sensing*, *63*(3), 283-296.

Schumm, S. A. (1993). River response to baselevel change: implications for sequence stratigraphy. *The Journal of Geology*, 279-294.

Shen, Z., Törnqvist, T. E., Autin, W. J., Mateo, Z. R. P., Straub, K. M., & Mauz, B. (2012). Rapid and widespread response of the Lower Mississippi River to eustatic forcing during the last glacial-interglacial cycle. *Geological Society of America Bulletin*, *124*(5-6), 690-704.

Slingerland, R., & Smith, N. D. (2004). River avulsions and their deposits. *Annu. Rev. Earth Planet. Sci.*, *32*, 257-285.

Strong, N., & Paola, C. (2008). Valleys that never were: time surfaces versus stratigraphic surfaces. *Journal of Sedimentary Research*, *78*(8), 579-593.

Swenson, J. B., & Muto, T. (2007). Response of coastal plain rivers to falling relative sea-level: allogenic controls on the aggradational phase.*Sedimentology*, *54*(1), 207-221.

Syvitski, J. P., & Lee, H. J. (1997). Postglacial sequence stratigraphy of Lake Melville, Labrador. *Marine Geology*, *143*(1), 55-79.

Syvitski, J. P., Overeem, I., Brakenridge, G. R., & Hannon, M. (2012). Floods, floodplains, delta plains—A satellite imaging approach. *Sedimentary Geology*, *267*, 1-14.

Vail, P. R. (1977). Seismic stratigraphy and global changes of sea-level, Part 4: Global cycles of relative changes of sea-level, Seismic stratigaphy-applications to hydrocarbon exploration. *Mem. Amer. Assoc. Petrol. Geol.*, (26), 83-97.

Van Heijst, M. W., & Postma, G. (2001). Fluvial response to sea-level changes: a quantitative analogue, experimental approach. *Basin Research*, *13*(3), 269-292.

Van Rijn, L. C. (1993). *Principles of sediment transport in rivers, estuaries and coastal seas* (Vol. 1006). Amsterdam: Aqua publications.

Vilks, G., & Mudie, P. J. (1983). Evidence for postglacial paleoceanographic and paleoclimatic changes in Lake Melville, Labrador, Canada. *Arctic and Alpine Research*, 307-319.

Vilks, G., Deonarine, B., & Winters, G. V. (1987). *Late quaternary marine geology of Lake Melville, Labrador*. Energy, Mines and Resources Canada.

Wood, L. J., Ethridge, F. G., & Schumm, S. A. (2009). The effects of rate of base-level fluctuation on coastal-plain, shelf and slope depositional systems: an experimental approach. *Sequence Stratigraphy and Facies Associations: Special Publication 18 of the IAS*, *100*, 43.

Wright, L. D. (1977). Sediment transport and deposition at river mouths: a synthesis. *Geological Society of America Bulletin*, *88*(6), 857-868.

Wright, L. D., & Coleman, J. M. (1973). Variations in morphology of major river deltas as functions of ocean wave and river discharge regimes. *AAPG Bulletin*, *57*(2), 370-398.